Plasma-based N_2 fixation into NO_x: Insights from modeling toward optimum yields and energy costs in a gliding arc plasmatron

Elise Vervloessem, Maryam Aghaei, Fatme Jardali, Neda Hafezkhiabani, Annemie Bogaerts

Research group PLASMANT, Department of Chemistry, University of Antwerp, Universiteitsplein 1, 2610 Antwerp, Belgium

Supporting information

Table of contents

Table S.8 Electron impact reactions implemented in the model for atomic and molecular nitrogen and oxygen species as well as NO_x species. The list includes vibrational excitation and de-excitation, electronic excitation and de-excitation, direct and dissociative ionization, dissociation, as well as direct and dissociative attachment reactions. These reactions are treated by energy-dependent cross sections when the rate coefficient is not specified. When indicated, rate coefficients are expressed in $cm^3\ s^{-1}$ or $cm^6\ s^{-1}$ for binary or ternary reactions, respectively.

Table S.9 Neutral-neutral reactions included in the model and the corresponding rate coefficient expressions. Tg is the gas temperature in K. .The rate coefficients are expressed in $cm^3\ s^{-1}$ or $cm^6\ s^{-1}$ for binary or ternary reactions, respectively. For certain reactions, the rate coefficients of the vibrationally excited species are determined according to the Fridman-Macheret model in which the activation energy is lowered by $\alpha\ E_v$, where α is the vibrational efficiency to lower the activation barrier and E_v is the vibrational energy. For those reactions, the α parameter is given in the last column.

Table S.10 Electron-ion recombination reactions included in the model and the corresponding rate coefficient expressions. Te is to the electron temperature in K and Tg is the gas temperature in K. The rate coefficients are expressed in $cm^3\ s^{-1}$ or $cm^6\ s^{-1}$ for binary or ternary reactions, respectively.

Table S.11 Ion-neutral reactions included in the model and the corresponding rate coefficient expressions. T_g is the gas temperature in K. For certain reactions, T_{ion} is the effective temperature of the reacting ion in K [26]. The rate coefficients are expressed in $cm^3\ s^{-1}$ or $cm^6\ s^{-1}$ for binary or ternary reactions, respectively.

Table S.12 Ion-ion reactions included in the model, the corresponding rate coefficient expressions and the references. T_g is the gas temperature in K. The rate coefficients are expressed in $cm^3\ s^{-1}$or $cm^6\ s^{-1}$ for binary or ternary reactions, respectively.

Table S.13 Optical transitions of N_2 and O_2 species. The rate coefficients are expressed in s^{-1}.

Table S. 14 Vibrational – vibrational exchanges and vibrational – translational relaxations for N_2 (as an example) and the rate coefficient expression.

1. Comparison with different plasma sources applied for NO_x formation

Table S.1 Yield and energy cost for NO_x formation in different plasma sources. They all operate at atmospheric pressure, unless mentioned otherwise. The HB process for NH_3 synthesis is also added, as benchmark.

Reactor	Yield [%]	Energy cost [MJ/mol]	Ref.
GAP	1.5 % NO_x	3.6 MJ/mol NO_x	This work
Electric arc (Birkeland – Eyde)	1 – 2 % NO	2.41 MJ/mol NO	[2]
Electric arc with water injection	2.41 % NO	3.5 MJ/mol NO	[3]
MW at reduced pressure with MoO_3 catalyst	6 % NO	0.84 MJ/mol NO	[4]
Pulsed MW at reduced pressure	6 % NO	0.60 MJ/mol NO	[5]
MW with magnetic field at reduced pressure	14 % NO	0.30 MJ/mol NO	[6]
DBD with γ – Al_2O_3 catalyst	0.5 % NO_x	18 MJ/mol NO_x	[7]
Shielded sliding discharge	0.1 % NO_x	15.4 MJ/mol NO_x	[8]
Pulsed milliscale GA	2 % NO_x	2.8 MJ/mol NO_x	[9]
Haber – Bosch	10 – 20 % NH_3[a]	0.48 MJ/mol[a]	[10]

a. Yield after one pass, depending on the specific plant, and energy cost of the whole process.

2. Details on the experimental setup

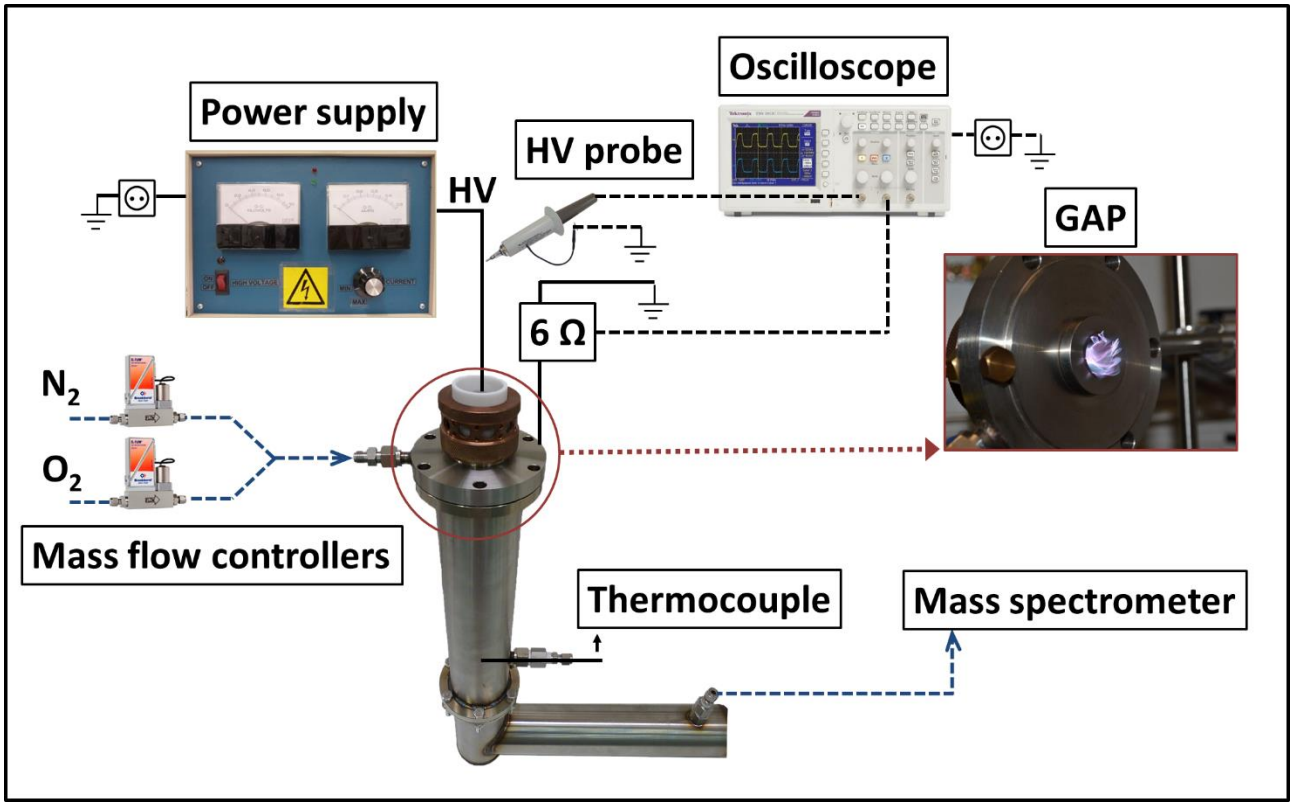

Figure S.1 Schematics of the entire experimental system used for the experimental procedure that was explained in the main paper.

For safety and environmental concerns, we have NO and NO_2 sensors in the lab to detect any probable leak. In addition, the whole experimental setup is placed in a separated fume hood, connected to special air filters to avoid introducing the exhaust gas to the open air and harming the environment.

3. 0D model description

A zero-dimensional (0D) chemical kinetics model was developed to solve a set of continuity equations (Eq. 2) for all individual species included in the model (see Table S.2), in order to obtain the species densities as a function of time:

$$\frac{dn_i}{dt} = \sum_j \left[\left(a_{ij}^R - a_{ij}^L \right) k_j \prod_l n_l^L \right] \tag{2}$$

n_i is the density of species i, a_{ij}^R and a_{ij}^L are the right and left stoichiometric coefficients for the following general reaction:

$$aA + bB\ (+\Delta H) \xrightarrow{k_j} cC + dD\ (+\Delta H) \tag{3}$$

With species i for reaction j. Here, A, B, C and D are the different species and a, b, c and d are their respective stoichiometric coefficients. ΔH represents the enthalpy of reaction j. The reaction rate coefficient, k_j, of the heavy particle reactions are either constant or dependent on the gas temperature and are expressed in $\mathrm{cm^3\ s^{-1}}$ or $\mathrm{cm^6\ s^{-1}}$ for two-body or three-body reactions, respectively. The rate coefficients of the electron impact reactions can depend on the electron temperature $\mathrm{T_e}$ (or the reduced electric field E/N, i.e., the electric field E divided by the number density of all neutral species N, usually expressed in $\mathrm{Td} = 10^{-21}\,\frac{\mathrm{V}}{\mathrm{m^2}}$). Most rate coefficients of electron impact reactions are calculated according to the following equation:

$$\mathrm{k_i} = \int_{\varepsilon_{\mathrm{th}}}^{\infty} \sigma_{\mathrm{i}}(\varepsilon)\mathrm{v}(\varepsilon)\mathrm{f}(\varepsilon)\mathrm{d}\varepsilon \tag{4}$$

ε is the electron energy (usually in eV), $\varepsilon_{\mathrm{th}}$ is the minimum threshold energy needed to induce the reaction, $\mathrm{v}(\varepsilon)$ the velocity of the electrons, $\sigma_{\mathrm{i}}(\varepsilon)$ is the cross section of collision i, and $\mathrm{f}(\varepsilon)$ is the electron energy distribution function (EEDF). We use the ZDPlasKin[11] code to solve the balance equations (Eq. 2) for all species, which has a built-in Boltzmann solver, BOLSIG+[12], to calculate the EEDF and the rate coefficients of the electron impact reactions based on a set of cross sections, the plasma composition, the gas temperature and the reduced electric field (E/N). The electric field (E) is calculated from a given power density, using the so-called local field approximation[13]:

$$\mathrm{E} = \sqrt{\frac{\mathrm{P}}{\sigma}} \tag{5}$$

P is the input power density (W $\mathrm{m^{-3}}$) and σ is the plasma conductivity (A $\mathrm{V^{-1}}$ $\mathrm{m^{-1}}$). The plasma conductivity is[13]

$$\sigma = \mathrm{e}\ \mathrm{n_e}\ \mu_{\mathrm{e}} \tag{6}$$

$\mathrm{n_e}$ is the electron number density and μ_{e} is the electron mobility.

The model is applied to the GAP reactor at exactly the same dimensions and operating conditions as in the experiments. A schematic diagram of the GAP, including the dimensions, is presented in Figure S.2. The arc plasma column inside the GAP is illustrated by the red rectangle. Because the gas enters the GAP reactor by tangential inlets, it follows a vortex flow pattern. As the outlet (anode) diameter is smaller than the reactor body (cathode part) (see Figure S.2a), the gas will first move upwards in a so-called forward vortex flow (indicated in Figure S.2a by the solid spiral). When the gas arrives at the top of the reactor, it will have lost most of its speed by friction and inertia. The gas will then travel downwards in a smaller so-called reverse vortex flow, which is more or less captured by the arc column (see dashed spiral in Figure S.2a).

The reverse vortex flow results in the stabilization of the arc column in the centre of the GAP, as was previously predicted by 3D fluid dynamics simulations.[14,15] The vast majority of the plasma conversion thus takes place in the column-shaped centre of the reactor. Since the plasma is confined

in the inner vortex of the gas flow, the plasma can be considered uniform and we can assume a constant power density applied to the gas during its residence time in the plasma. This is convenient for the 0D model, which does not include spatial variations or transport. However, the calculated temporal dependence of the species densities can be transformed into a spatial dependence through the reactor by means of the gas flow rate[16,17] (see Figure S.2b). The arc plasma column is thus considered as a plug flow reactor, where the plasma characteristics vary as a function of distance travelled by the gas within a certain residence time, in the same way as they would vary as a function of time in a batch reactor. 2D fluid dynamics simulation results of Trenchev et al. for a GAP in argon [14,15] revealed that the arc radius is typically around 1 mm. However, the temperature just outside this arc region is still high enough to induce plasma, especially in a molecular plasma where vibration-translation (VT) relaxation causes gas heating. Therefore, we assumed an arc radius of 2 mm in our simulations. Combined with the length of the cathode (10.20 mm) and anode (16.30 mm) and the inlet of 3 mm (see Figure S.1), this yields a plasma volume of 0.37 cm^3. These input data were also successfully used in [18–20].

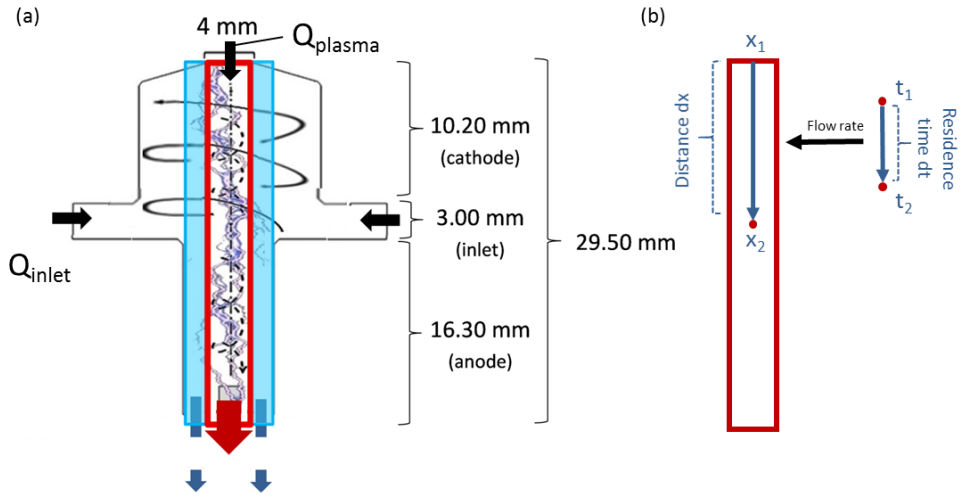

Figure S.2 (a) Schematic illustration of the GAP, indicating its dimensions as well as the outer vortex (solid spiral) and the inner (reverse) vortex (dashed spiral). The red frame indicates the plasma arc column, while the blue part indicates the region where the gas leaves the reactor without being treated. (b) Schematic of the 0D modeling approach in which the time dependency is translated into a spatial dependency by means of the gas flow rate.

We assume a constant temperature of 3000 K as input in our model, based on 3D fluid dynamics simulations[14,15]. Note that the calculated value was obtained for CO_2, and the experimental value for pure N_2, but not for N_2/O_2 gas mixtures. We expect the temperature profiles to be similar as they are all molecular gasses, as they experience the same mechanisms causing gas heating. We can also safely assume that the gas is already heated up to 3000 K when it enters the inner vortex, where the majority of the conversion takes place, so this is why the temperature profile starts at 3000 K and is kept constant. Gröger et al. have measured a gas temperature of 5000 K in our GAP operating in pure N_2.[21] This high temperature, however, likely originates from the hot cathode spot, so we think that 3000 K is a better estimate of the gas temperature inside the arc.

As initial conditions in the plasma, we start with a fixed electron density of 10^{10} cm^{-3}, considering only N_2 and O_2 molecules, including their vibrationally excited equivalents, N_2^+ and O_2^+ ions and electrons. We assume quasi-neutrality by setting the electron density equal to the sum of the densities of the N_2^+ and O_2^+ ions, according to their fraction in the inlet mixture. In addition, we assume a Boltzmann distribution for all vibrationally exited species, at a temperature of 3000 K. The sum of the initial densities of N_2, $N_2(v_x)$ and N_2^+ ions amounts to the total density that N_2 would have according to its initial fraction in the feed. Similarly, the sum of the initial densities of O_2, $O_2(v_x)$ and O_2^+ ions is according to the O_2 fraction in the feed.

Vibrational excitation of N_2 is promoted in the GAP and is advantageous for more energy-efficient dissociation of N_2, because it can help to overcome the reaction energy barrier of the Zeldovich mechanism.[22,23] Therefore, special attention is given to the vibrational levels: 24 vibrational levels for N_2 and 15 levels for O_2 were implemented in the model. The species taken into account in the model are listed in Table S.2. This includes neutral molecules in the ground, vibrationally and electronically excited states, various radicals, positive and negative ions, and electrons. In total, 1195 different electron impact, 435 neutral-neutral, 523 ion-neutral and 48 ion-ion chemical reactions are included, as well as 2478 vibrational-vibrational (VV) exchanges and vibrational-translational (VT) relaxations between $N_2 – N_2$, $O_2 – O_2$, and $N_2 – O_2$, and between $O_2 – O_2$, $N_2 – N_2$, $N_2 – N$ and $O_2 – O$, for all vibrational levels. The reaction set of in reference [24] was revised and used, but with the addition of $N_2 – O_2$ VV exchanges and $N_2 – N$ and $O_2 – O$ VT relaxations. The latter processes do not significantly influence the NO_x formation at the conditions under study, but were included for the sake of completeness. The $N_2 – O_2$ VV exchanges are demonstrated to be very important (cf. Figure 6 in the main paper). The vibrational levels of NO and NO_2 are not included, because of lack of data on their vibrational kinetics in literature. All reactions are listed under section 9.

Table S.2 Species included in the model

N_2 species	
Neutral ground state molecules	N_2
Ions	N^+, N_2^+, N_3^+, N_4^+
Vibrationally excited molecules	$N_2(v_1 - v_{24})$
Electronically excited molecules or atoms	$\mathrm{N_2(A^3\Sigma_u^+)}, \mathrm{N_2(B^3\Pi_g)}$, $\mathrm{N_2(C^3\Pi_u)}$ and $\mathrm{N_2\ (a'^1\Sigma_u^-\ )}, N(2D), N(2P)$
Radicals	N
N_xO_y species	
$NO, N_2O, NO_2, NO_3, N_2O_5, N_2O_3, N_2O_4, NO^+, N_2O^+, NO_2^+, NO^-, N_2O^-, NO_2^-, NO_3^-, O_2^+N_2$	
O_2 species	

Neutral ground state molecules	O_2, O_3
Ions	$O^-, O_2^-, O_3^-, O_4^-, O^+, O_2^+, O_4^+$
Vibrationally excited molecules	$O_2\ (v_1 - v_{15})$
Electronically excited molecules or atoms	$O\ (1D), O\ (1S), \mathrm{O_2(a^1\Delta)}$, $\mathrm{O_2(b^1\Sigma^+)}$ and a combination of three states, i.e. $\mathrm{O_2(A^3\Sigma^+, C^3\Delta, c^1\Sigma^-)}$ at a threshold energy of 4.5 eV.
radicals	O

The product yield, also reported in the main paper, is defined as:

$$\mathrm{Y_x = Y_{x,arc} \cdot f} \tag{7}$$

where f is the fraction of gas passing through the plasma arc and is defined as:

$$\mathrm{f = \frac{Q_{plasma}}{Q_{inlet}}} \tag{8}$$

where $\mathrm{Q_{inlet}}$ is the flow rate at the inlet of the rector and $\mathrm{Q_{plasma}}$ is the flow rate of the gas in the plasma region (red frame in Figure S.1(a)). In a GAP operating at atmospheric pressure, only14.8% of the gas flows through the plasma region and the remaining 85.2% is assumed in this model to leave the reactor without being treated. $\mathrm{Y_{x,arc}}$ corresponds to the product yield in the plasma arc region and is defined as:

$$\mathrm{Y_{x,arc} = \frac{n_x}{n_0} \cdot 100\%} \tag{9}$$

where $\mathrm{n_x}$ is the density ($\mathrm{cm^{-3}}$) of species x, for example NO or $\mathrm{NO_2}$ and $\mathrm{n_0}$ is the initial gas density.

4. Detailed experimental results

The experimental procedure consists of stabilizing the plasma for 15 minutes, followed by online continuous mass spectrometry measurements, and at the same time recording the plasma voltage and current in order to calculate the plasma power, and finally a cool down and flush period of 30 minutes with the next gas mixture. Each condition is repeated for three times and the results shown below are, thus, the average of these three measurements.

4.1Plasma power measurement

To calculate the plasma power, we measured the voltage and current passing through the arc. For this purpose, an oscilloscope (Tektronix TDS2012C) was used. The voltage was measured using a high voltage probe (Testec) connected to the cathode, the ground wire and channel 1 of the oscilloscope. The current was measured over an external resistor box by a wire connection to the second channel of the oscilloscope, using $\mathrm{I = V/R}$ with the resistance of the resistor box being 6 Ohm. The potential and current over a certain period of time were used to calculate the plasma power with the following formula:

$$P_{plasma} = \frac{1}{T}\int_{0}^{t=T} V_{plasma} \cdot I_{plasma} dt \quad (1)$$

Also, several pressure sensors were placed along the gas circuit to monitor the correct working of the setup during the experiments. Table S.3 shows the average plasma power measured by the oscilloscope, as well as the specific energy input (SEI) for each N_2/O_2 ratio with a total flow rate of 10 L/min. The error values are also indicated in Table S.3.

Table S.3 Average plasma power for different N_2/O_2 ratios and different flow rates.

N_2/O_2 ratio	Total flow rate [L/min]	Flow rate-error	Average plasma power [W]	Power-error	SEI [J/L]	SEI-error
9/1	10.00	0.07	365	9	2190	57
8/2	10.00	0.07	369	28	2214	171
7/3	10.00	0.07	379	11	2274	69
6/4	10.00	0.07	409	25	2454	151
5/5	10.00	0.07	415	11	2492	71
4/6	10.00	0.07	434	23	2606	139
3/7	10.00	0.07	437	13	2624	83
2/8	10.00	0.07	458	12	2748	75
1/9	10.00	0.07	381	33	2289	201
8/2	8.000	5.01	490	5	3679	48
8/2	12.000	17.84	390	18	1951	90
8/2	14.000	32.08	428	16	1837	70
8/2	16.000	25.56	548	26	2057	97
8/2	18.000	29.70	390	30	1299	99
8/2	20.000	11.12	490	11	1471	34
8/2	22.000	33.85	364	34	993	92
8/2	25.000	11.55	476	12	1144	28
8/2	30.000	12.89	375	13	750	26

4.2 Gas analysis and product concentrations

The output gas composition was analyzed online by a mass spectrometer (Hiden Analytical Limited, QGA Pro v1.6). The mass spectrometer was calibrated separately with a mixture of 867 ppm NO_2 in He and 976 ppm NO in He. For both NO and NO_2, a response factor was calculated and used to determine the concentration of the detected products, which is 1696 for NO and 313 for NO_2. Table S.2 shows the NO and NO_2 concentrations (ppm) before calibration, the calibrated concentrations (ppm), as well as the product selectivity for different N_2 and O_2 gas mixtures.

Table S.4 NO and NO_2 concentrations (ppm) before calibration, calibrated concentrations (ppm) and product selectivity. We also checked for N_2O and N_2O_4 but their concentrations were below the detection limit.

N_2/O_2 ratio	NO concentration [a.u.]	Calibrated-NO [ppm]	NO_2 concentration	Calibrated-NO_2 (ppm)	NO selectivity [%]	NO_2 selectivity [%]
9/1	$7.61x10^{-8}$	$1.29x10^{-4}$	$1.73x10^{-8}$	$5.41x10^{-6}$	95.97	4.03
8/2	$8.04x10^{-8}$	$1.36x10^{-4}$	$4.26x10^{-8}$	$1.33x10^{-5}$	91.09	8.91
7/3	$7.90x10^{-8}$	$1.34x10^{-4}$	$6.04x10^{-8}$	$1.89x10^{-5}$	87.63	12.37
6/4	$7.61x10^{-8}$	$1.29x10^{-4}$	$8.03x10^{-8}$	$2.51x10^{-5}$	83.70	16.30
5/5	$7.24x10^{-8}$	$1.23x10^{-4}$	$8.43x10^{-8}$	$2.64x10^{-5}$	82.31	17.69
4/6	$6.57x10^{-8}$	$1.11x10^{-4}$	$8.17x10^{-8}$	$2.56x10^{-5}$	81.33	18.67
3/7	$6.20x10^{-8}$	$1.05x10^{-4}$	$7.90x10^{-8}$	$2.47x10^{-5}$	80.96	19.04
2/8	$5.45x10^{-8}$	$9.24x10^{-5}$	$7.03x10^{-8}$	$2.20x10^{-5}$	80.77	19.23
1/9	$4.04x10^{-8}$	$6.85x10^{-5}$	$4.52x10^{-8}$	$1.41x10^{-5}$	82.89	17.11

4.3Energy measurements

Table S.5 Measured energy cost (EC) with the corresponding error values for different N_2/O_2 ratios.

N_2/O_2 ratio	EC	EC-error
9/1	$3.99x10^{6}$	$0.10x10^{6}$
8/2	$3.62x10^{6}$	$0.28x10^{6}$
7/3	$3.64x10^{6}$	$0.11x10^{6}$
6/4	$3.90x10^{6}$	$0.24x10^{6}$
5/5	$4.09x10^{6}$	$0.12x10^{6}$
4/6	$4.66x10^{6}$	$0.25x10^{6}$
3/7	$4.95x10^{6}$	$0.16x10^{6}$
2/8	$5.88x10^{6}$	$0.16x10^{6}$
1/9	$6.78x10^{6}$	$0.59x10^{6}$

5. Raw data from the model

Table S.6 Calculated yield of NO and NO_2 and energy consumption (EC) as a function of N_2 fraction in the feed gas, for a gas flow rate of $10\ L\ min^{-1}$, a pressure of 1.25 bar and a power ranging from 365 to 458 W (slightly varying for different gas composition; see Table S.3).

N_2 [%]	NO [%]	NO_2 [%]	EC [MJ/mol]
10	0.48	0.06	11.44
20	0.76	0.08	7.98
30	1.01	0.10	5.77

40	1.30	0.12	4.49
50	1.44	0.12	3.91
60	1.49	0.11	3.75
70	1.44	0.10	3.63
80	1.35	0.07	3.81
90	1.11	0.04	4.66

Table S.7 Calculated density of N_2O, N_2O_4, NO_3, N_2O_5 and N_2O_3 as a function of N_2 fraction in the feed gas, for a gas flow rate of $10\ L\ min^{-1}$*, a pressure of 1.25 bar and a power ranging from 365 to 458 W (slightly varying for different gas compositions; see Table S.3).*

N_2 [%]	**N_2O [cm^{-3}]**	**N_2O_4 [cm^{-3}]**	**NO_3 [cm^{-3}]**	**N_2O_5 [cm^{-3}]**	**N_2O_3 [cm^{-3}]**
10	6.81×10^{12}	1.16×10^{5}	5.22×10^{13}	1.02×10^{5}	8.62×10^{7}
20	1.66×10^{13}	2.53×10^{5}	8.11×10^{13}	2.34×10^{5}	2.04×10^{8}
30	2.81×10^{13}	3.76×10^{5}	9.62×10^{13}	3.39×10^{5}	3.31×10^{8}
40	4.58×10^{13}	5.29×10^{5}	1.10×10^{14}	4.59×10^{5}	5.05×10^{8}
50	5.75×10^{13}	5.47×10^{5}	1.04×10^{14}	4.44×10^{5}	5.68×10^{8}
60	6.54×10^{13}	4.86×10^{5}	9.04×10^{13}	3.62×10^{5}	5.55×10^{8}
70	6.58×10^{13}	3.49×10^{5}	6.78×10^{13}	2.30×10^{5}	4.55×10^{8}
80	6.49×10^{13}	2.11×10^{5}	4.40×10^{13}	1.16×10^{5}	3.31×10^{8}
90	5.37×10^{13}	6.86×10^{4}	1.75×10^{13}	2.64×10^{4}	1.55×10^{8}

6. Benchmarking the energy cost of our GAP reactor: Chi parameter

The various plasma sources listed in Table S.6 are all different in structure, geometry and excitation modes, and they potentially have different chemical reaction pathways for NO_x production. Therefore, Pei et al. proposed a dimensionless parameter (χ) to compare different plasma set-ups [1].:

$$\chi = \frac{\bar{E} \cdot \bar{T}}{\bar{E}_r \cdot \bar{T}_r} \quad (4)$$

Where $\bar{E}$ and $\bar{T}$ are the average electric field and average gas temperature of a specific plasma type, and $\bar{E}_r$ and $\bar{T}_r$ are reference values chosen to normalize these parameters at 1.43 kV/cm and 1800 K, respectively.

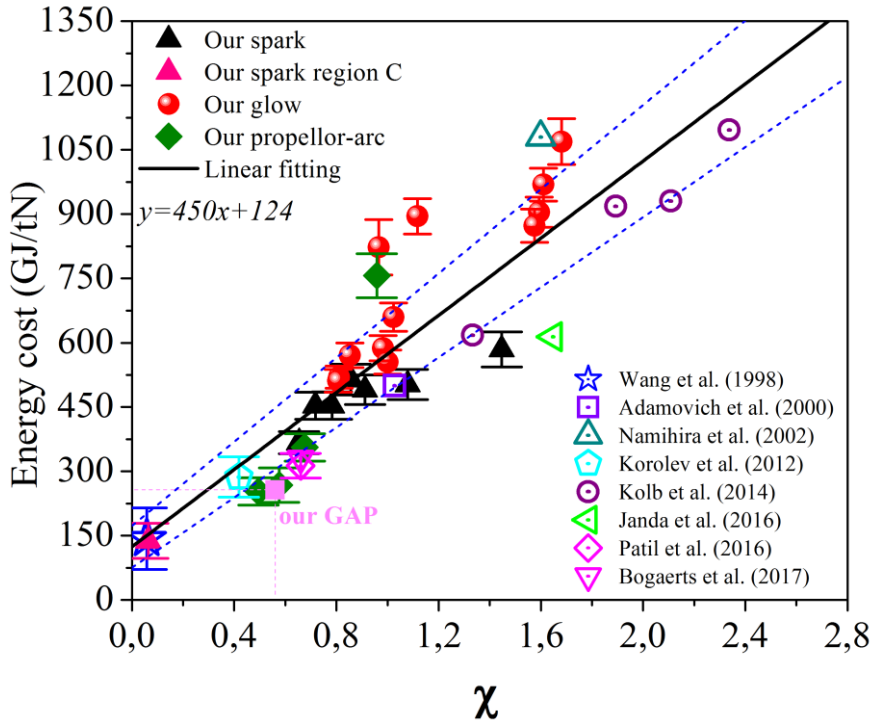

Figure S.3 Energy cost for NO_x production as a function of the χ parameter, compared to the reported works from literature and the results of Pei et al. using different plasma sources. The figure is adapted from ref.[1] with the permission from the authors. The χ parameter of our GAP is plotted in pink (for the conditions described in the section below).

They observed that the energy cost (reported per unit of reactive N, expressed in units of GJ/tN) increases linearly with χ for different plasma types evaluated, and thus they concluded that χ can give a good indication of the energy cost performance of a specific plasma set-up for NO_x production. Based on the calculated gas number density of 3.02 x 10^{18} cm^{-3} and an average reduced electric field of 16 Td, we estimate for our GAP an average electric field of 0.48 kV/cm, while the average gas temperature in the arc should be around 3000 K[15]. This yields a χ value of 0.56. The minimum energy cost in GJ/tN in our GAP is 257 GJ/tN. If we would add this data point to the figure in ref.[25] (see pink square on Figure S.3), our EC is in the range of what is predicted by the linear dependency between EC and χ.

7. Reaction analysis

The net rates for the production or loss of NO and NO_2, discussed in the main paper, are plotted as a function of the N_2 fraction in the feed gas in Figure S.4. As NO_2 is always formed from NO, the main processes for the formation and loss of NO_2 are also included in this figure, though formulated as an NO loss instead of an NO_2 formation process. For the sake of clarity, we have plotted processes N1 and N5 on the right y-axis, which is 10 times larger than the left y-axis, so that the evolution of the rates of the Zeldovich processes (N2 and N3) is clearly visible. The Zeldovich mechanism (N2 and N3) as a function of the N_2 fraction in the feed is discussed in section 3.4 of the main paper. As seen in Figure S.4, N1 is the dominant NO formation reaction at N_2 fractions below 60 %. At higher N_2 fractions, reaction N2 becomes more important, as there is less O_2 available. NO is rapidly converted

into NO_2 through N4 (pink curve in Figure S.4). Its rate drops with increasing N_2 fraction, as this process requires atomic O. Next, NO_2 is converted back to NO through N1 (red curve) and N4 (purple curve), which are the two main loss channels for NO_2.

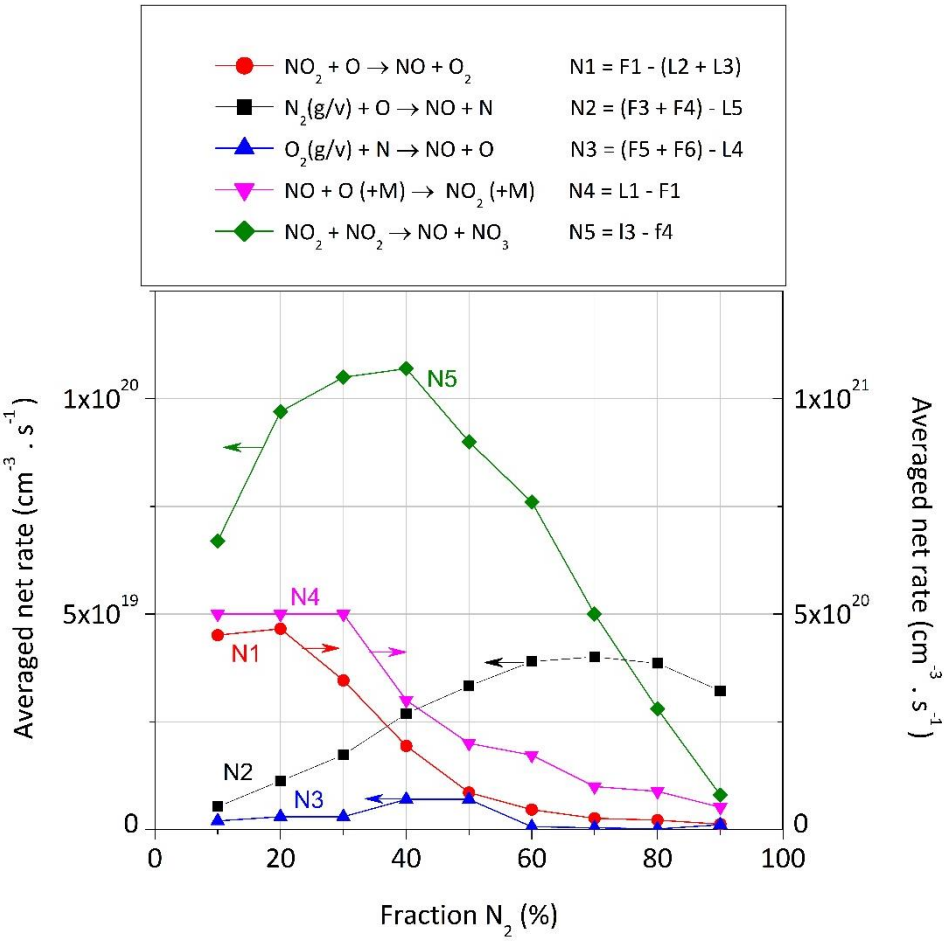

Figure S.4 Net rates of the most important formation and loss process of NO (and NO_2) as a function of the N_2 fraction in the feed gas, at the same condition as in Figure 1 in the main paper.

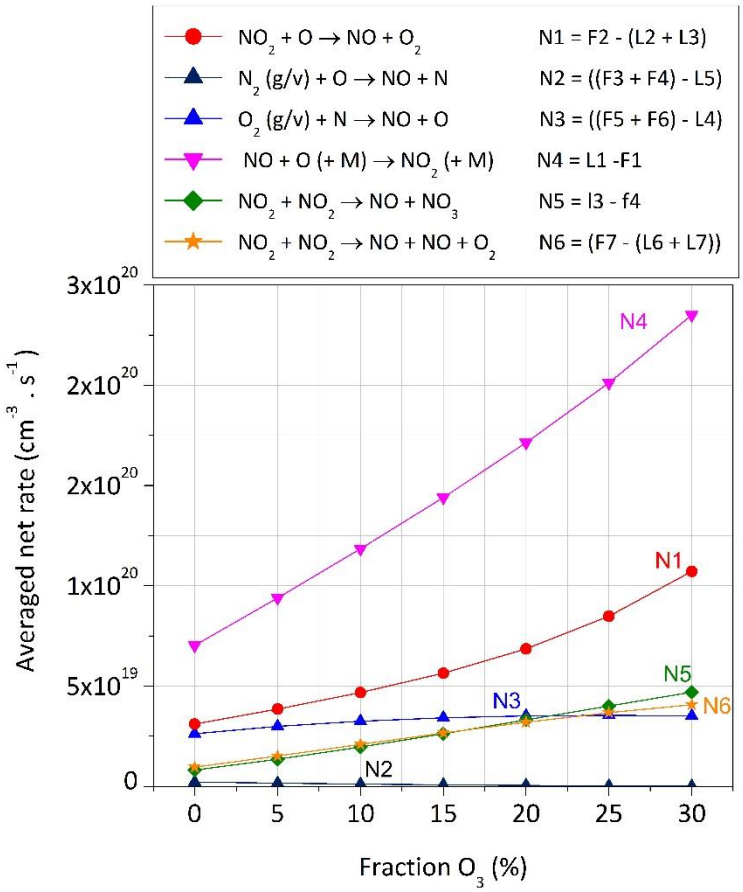

Figure S.5 Net rates of the most important formation and loss processes of NO as a function of the O_3 fraction in the feed gas at a N_2/O_2 ratio of 80/20, flow rate of 10 L min^{-1} and a power of 400 W.

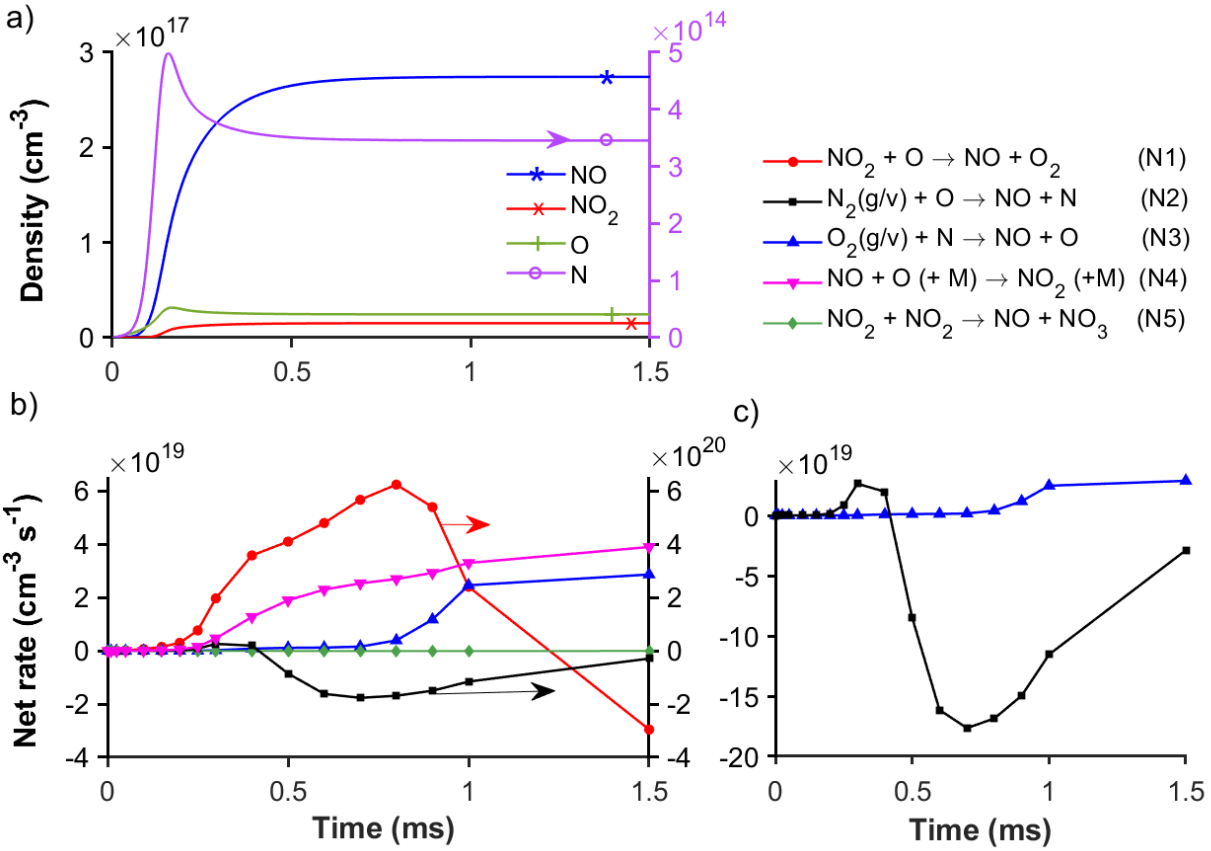

Figure S.6: Calculated number densities of NO, NO_2, O and N (a), and net rates of the main reactions as function of residence time until steady state (b), for an 80/20 N_2/O_2 mixture at 1.25 bar, 10 L min^{-1} and 415 W. The same figure for the full residence time (15 ms) can be found in Figure S.7. Panel (c) shows reactions N2 and N3 in detail.

The NO, NO_2, N and O densities reach steady state already in the first 0.5 ms, which can be explained as follows. First, the N atoms are predominantly (99.98 %) formed through electron impact dissociation of N_2(g/v) (see peak in Figure S.6a: purple curve). The N atoms are partially consumed in the Zeldovich mechanism (Figure S.6b and c: blue curve, N3) with the formation of NO. Similarly, the O atoms are formed through direct electron impact dissociation and collision with electronically excited N_2 molecules (as discussed of the main paper) and partially consumed through the second step of the Zeldovich mechanism (Figure S.6b and c: black curve, N2). Once NO is formed, it is either (1) converted into NO_2 (Figure S.6b: pink curve, N4), or (2) destroyed through the backward reaction of N2. Indeed, the rate of N2 becomes negative around 0.5 ms (see Figure S.6b and c: black curve). In case it had been converted into NO_2 it is partially converted back into NO (Figure S.6b: red curve, N1). Under these conditions the backward reaction of N3 is not promoted, and the net reaction rate is in favor of NO production throughout the entire residence time. On the other hand, the net rate of N2 is in favor of NO production before 0.5 ms, but decreases after 0.5 ms in favor of NO desctruction. This limits the NO production.“

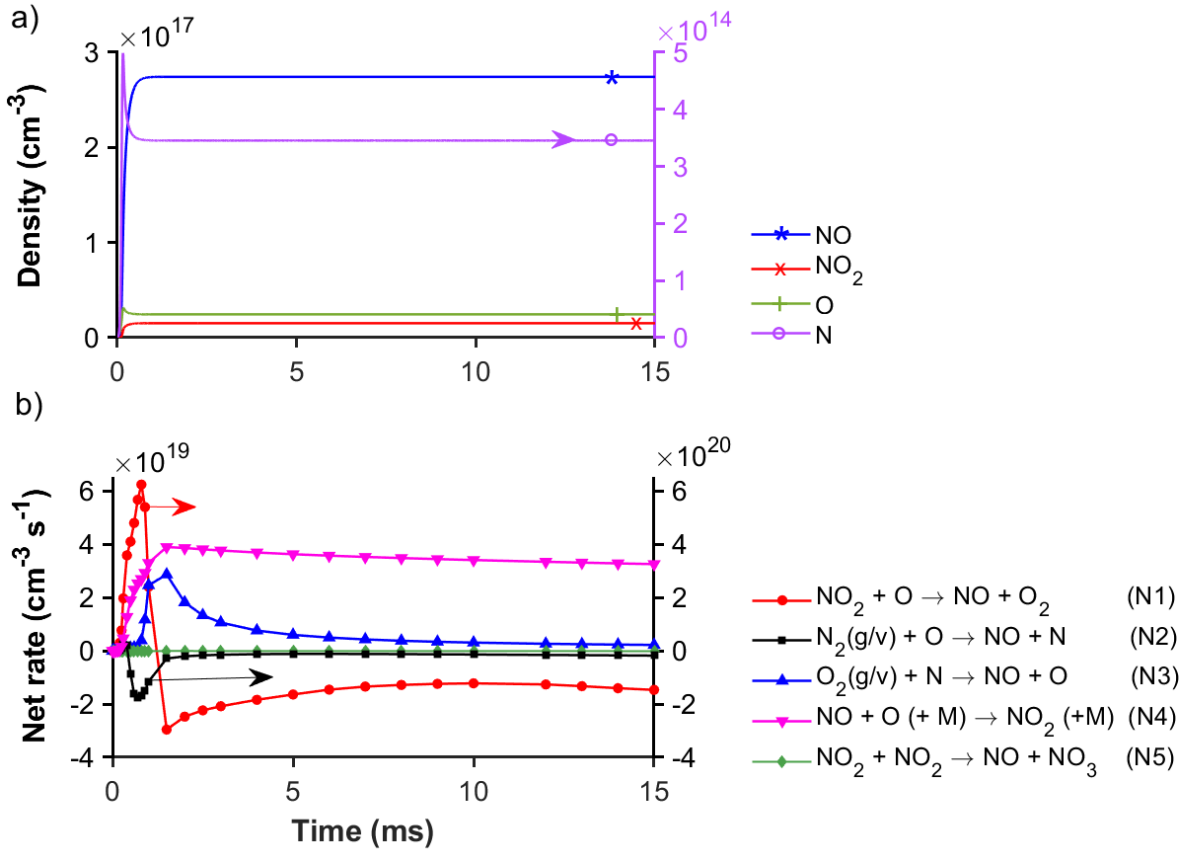

Figure S.7 Calculated number densities of NO, NO_2, O and N (a), and net rates of the main reactions as function of the residence time (b), for an 80/20 N_2/O_2 mixture at 1.25 bar, 10 L min^{-1} and 415 W.

8. VDFs of N_2 and O_2

In this section we give a more elaborate description and discussion of the VDF of N_2 an O_2 to support our discussion in the main paper.

The chemistry set we developed for this model includes an extensive description of the vibrational kinetics of both N_2 and O_2. A simple measure of the degree of vibrational excitation is the vibrational temperature, calculated according to:

$$T_v = \frac{1}{m}\sum_1^m -\frac{(E_i - E_{i-1})}{\ln(\frac{n_i}{n_{i-1}})} \qquad (5)$$

With m being an integer corresponding to the number of vibrational levels taken into account in the calculation of the vibrational temperature, E_i is the vibrational energy of the ith level and n_i is the density of the molecule at the ith level. The vibrational temperature, based on the 24 vibrational levels of N_2 included in the model, is calculated to be 3325 K. This is slightly higher than the gas temperature in the arc, which is expected to be around 3000 K, based on 2D fluid dynamics modeling[15], and taken as constant in our model (see section 4 above). The vibrational temperature of O_2 is calculated to be 2632 K, based on the 15 vibrational levels of O_2 taken into account in the model. Hence, this is somewhat lower than the vibrational temperature of N_2. Indeed, even though the reaction rate

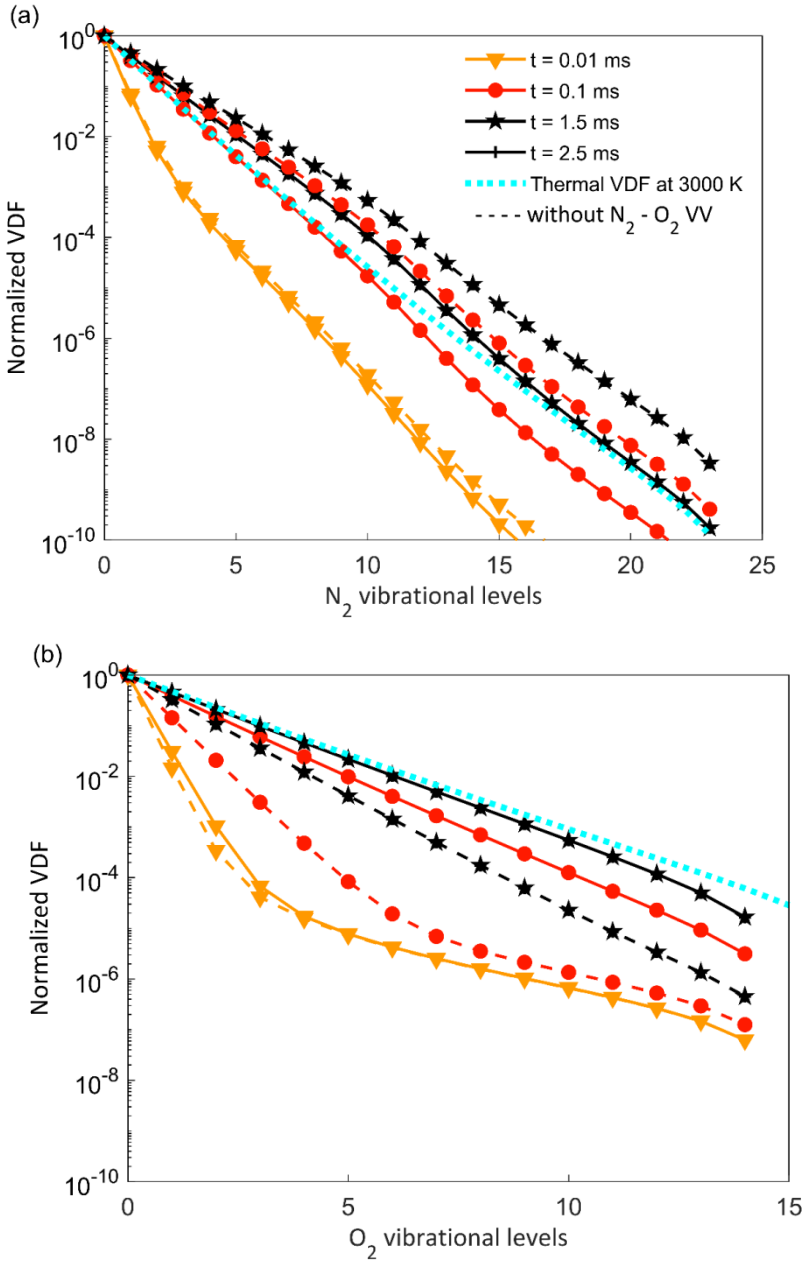

Figure S.8 Normalized vibrational distribution function (VDF) of N_2 (a) and O_2 (b) at different times in the plasma for a 50/50 N_2/O_2 plasma, and at the same conditions as in Figure 1. The solid and dashed curves represent the VDFs of a chemistry set that includes and excludes N_2 –O_2 VV exchanges, respectively (see next section). The black full lines (representing t = 1.5 and 2.5 ms) are on top of one another, as well as the black dashed lines, indicating that the VDFs of N_2 and O_2 reach steady state already after 1.5 ms. For comparison, the thermal VDF at 3000 K is also plotted as a dotted blue curve.

constants of N_2 – N_2 vibrational ladder climbing (by vibrational-vibrational (VV) exchanges) are five times lower than for O_2 – O_2 vibrational ladder climbing, the reaction rate constants of the different depopulation mechanisms of the O_2 vibrational levels (i.e., by vibrational-translational (VT) exchanges: O_2 – O VT, O_2 – N_2 VT and O_2 – O_2 VT) are higher than the rate constants of the same

mechanisms for the N_2 vibrational levels, resulting in easier depopulation of the O_2 vibrational levels. In Figure S.8, we plot the vibrational distribution function (VDF), i.e., normalized density of the vibrational levels, of N_2 (panel a, solid lines) and O_2 (panel b, solid lines), at different times in the

plasma, as well as the thermal distribution of N_2 and O_2 at 3000 K (dotted, light blue curves). The VDF of N_2 is in thermal equilibrium for the majority of the residence time. At short residence time (t = 0.01 ms), the vibrational temperature is much lower than 3000 K, but the population quickly builds up, to a vibrational temperature above 3000 K at 1.5 ms. The VDF of O_2 shows an overpopulation of the higher vibrational levels at short residence times (t = 0.01 ms), but after 1.5 ms, the VDF also becomes in equilibrium, with a temperature slightly below the gas temperature of 3000 K. Both VDFs reach a quasi-steady state after 1.5 ms. Although the VDFs are thermal, the higher vibrational levels are nevertheless sufficiently populated to facilitate dissociation, as illustrated in Figure 3 and Table 1 in the main paper. Moreover, the vibrational levels in our GAP are more populated than in other set-ups, like a classical GA, where the VDF drops significantly for the higher vibrational levels.[24]

9. Chemistry set

The chemistry set used in this model is based on the work done by Wang et al.[24], but revised and updated. For instance, the set contains a more elaborate description of the vibrational kinetics of N_2 and O_2 (i.e. $N_2 - O_2$ vibrational-vibrational (VV) exchanges and $N_2 - N$ and $O_2 - O$ vibrational-translational (VT) relaxations, see Table S.13). 24 vibrational levels for N_2 and 15 levels for O_2 were implemented in the model. The species taken into account in the model are listed in Table S.5 above. This includes neutral molecules in the ground state, vibrationally and electronically excited states, various radicals, positive and negative ions, and electrons. Table S.7 lists all electron impact reactions. Most of these reactions are treated by energy-dependent cross sections. Table S.8 lists the neutral-neutral reactions and the corresponding rate-coefficient expressions. For certain reactions, the rate coefficients of the vibrationally excited species are determined according to the Fridman-Macheret model in which the activation energy is lowered by $\alpha\, E_v$, where α is the vibrational efficiency to lower the activation barrier and E_v is the vibrational energy. For those reactions, the α parameter is given in the last column of Table S.8. Tables S.9 to S.11 list the electron-ion recombination, the ion-neutral and the ion-ion reactions and the corresponding rate coefficients, respectively. Table S.12 displays the optical transitions

Table S.8 Electron impact reactions implemented in the model for atomic and molecular nitrogen and oxygen species as well as NO_x species. The list includes vibrational excitation and de-excitation, electronic excitation and de-excitation, direct and dissociative ionization, dissociation, as well as direct and dissociative attachment reactions. These reactions are treated by energy-dependent cross sections when the rate coefficient is not specified. When indicated, rate coefficients are expressed in $cm^3\ s^{-1}$ or $cm^6\ s^{-1}$ for binary or ternary reactions, respectively.

Reaction	Rate Coefficient	Ref.	Note
$e^- + N_2 \leftrightarrow e^- + N_2(v)$		26	
$e^- + N_2(v) \leftrightarrow e^- + N_2(v')$		26	
$e^- + N_2(g,v) \rightarrow e^- + N_2(E_x)$		27	a, b, c
$e^- + N_2(E_x) \rightarrow e^- + N_2$		27	b
$e^- + N_2(g,v) \rightarrow 2e^- + N_2^+$		28	a
$e^- + N_2(E_x) \rightarrow 2e^- + N_2^+$		28	b
$e^- + N \rightarrow 2e^- + N^+$		27	
$e^- + N_2(g,v) \rightarrow 2e^- + N^+ + N$		29	a
$e^- + N_2(g,v) \rightarrow e^- + N + N$		27	a, c
$e^- + N_2(E_x) \rightarrow e^- + N + N$		27	b
$e^- + N \rightarrow e^- + N(E_x)$		27	d
$e^- + O_2 \leftrightarrow e^- + O_2(v)$		26	
$e^- + O_2(v) \leftrightarrow e^- + O_2(v')$		30	

$e^- + O_2(g,v) \rightarrow e^- + O_2(E_x)$		27	a, c, e
$e^- + O_2(E_x) \rightarrow e^- + O_2$		27	e
$e^- + O_2(g,v) \rightarrow 2e^- + O_2^+$		28	a, c
$e^- + O_2(E_x) \rightarrow 2e^- + O_2^+$		31	e
$e^- + O \rightarrow 2e^- + O^+$		27	
$e^- + O_2(g,v) \rightarrow 2e^- + O + O^+$		32	a, c
$e^- + O_2(E_x) \rightarrow 2e^- + O + O^+$		32	e
$e^- + O_3 \rightarrow 2e^- + O + O_2^+$		33	
$e^- + O_3 \rightarrow e^- + O^+ + O^- + O$		27	
$e^- + O_2(g,v) \rightarrow e^- + O + O$		27	a
$e^- + O_3 \rightarrow e^- + O_2 + O$		33	
$e^- + O_2(g,v) \rightarrow O + O^-$		27	a, c
$e^- + O_2(g,v) + M \rightarrow O_2^- + M$		34	a, c, f
$e^- + O_3 \rightarrow O^- + O_2$		28	
$e^- + O_3 \rightarrow O + O_2^-$		28	
$e^- + O_3 + M \rightarrow O_3^- + M$	5×10^{-31}	35	f
$e^- + O + M \rightarrow O^- + M$	1×10^{-31}	36	f
$e^- + NO \rightarrow 2e^- + NO^+$		37	
$e^- + NO_2 \rightarrow 2e^- + NO_2^+$		38	
$e^- + N_2O \rightarrow 2e^- + N_2O^+$		39	
$e^- + N_2O \rightarrow e^- + N_2 + O$		40	
$e^- + N_2O \rightarrow e^- + N_2 + O(1D)$		40	
$e^- + N_2O \rightarrow e^- + NO + N$		40	
$e^- + NO \rightarrow O^- + N$		37	
$e^- + N_2O \rightarrow N_2 + O^-$		39	
$e^- + NO_2 \rightarrow NO_2^-$	1×10^{-11}	41	
$e^- + NO_2 \rightarrow O^- + NO$	1×10^{-11}	42	
$e^- + NO + M \rightarrow NO^- + M$	8×10^{-31}	42	f
$e^- + N_2O + M \rightarrow N_2O^- + M$	6×10^{-33}	42	f

[a] For any species indicated with (g,v), g and v stand for its ground and vibrationally excited state, respectively.

[b] $N_2(E_x)$ represents the electronically excited states: $N_2(A^3\Sigma_u^+)$, $N_2(B^3\Pi_g)$, $N_2(C^3\Pi_u)$ and $N_2\left(a'^1\Sigma_u^-\right)$.

[c] The cross sections of the reactions involving excited species on the left hand side are shifted over the difference in the threshold energies.

[d] $N(E_x)$ represents the electronically excited states of atomic N: $N(2D)$ and $N(2P)$.

[e] $O_2(E_x)$ represents the electronically excited states: $O_2(a^1\Delta)$, $O_2(b^1\Sigma^+)$ and a combination of three states, i.e. $O_2(A^3\Sigma^+, C^3\Delta, c^1\Sigma^-)$ at a threshold energy of 4.5 eV.

[f] M represents any neutral species.

Table S.9 Neutral-neutral reactions included in the model and the corresponding rate coefficient expressions. Tg is the gas temperature in K. .The rate coefficients are expressed in $cm^3\ s^{-1}$ or $cm^6\ s^{-1}$ for binary or ternary reactions, respectively. For certain reactions, the rate coefficients of the vibrationally excited species are determined according to the Fridman-Macheret model in which the activation energy is lowered by $\alpha\ E_v$, where α is the vibrational efficiency to lower the activation barrier and E_v is the vibrational energy. For those reactions, the α parameter is given in the last column.

Reaction	**Rate coefficient**	**Ref.**	**Note**
$N_2(g,v) + M \rightarrow N + N + M$	$8.37 \times 10^{-4} \times \left(\frac{T_g}{298}\right)^{-3.5} \times \exp\left(-\frac{113710}{T_g}\right)$	43	a, b $\alpha = 1$
$N + N + M \rightarrow N_2 + M$	$1.38 \times 10^{-33} \times \exp\left(\frac{502.978}{T_g}\right)$	44	b
$N + N \rightarrow N_2^+ + e^-$	$2.7 \times 10^{-11} \times \exp\left(-\frac{6.74\times10^4}{T_g}\right)$	42	
$N + N + N \rightarrow N_2(A^3\Sigma_u^+) + N$	1.0×10^{-32}	42	
$N + N + N \rightarrow N_2(B^3\Pi_g) + N$	1.4×10^{-32}	42	
$N + N + N_2 \rightarrow N_2(A^3\Sigma_u^+) + N_2$	1.7×10^{-33}	42	
$N + N + N_2 \rightarrow N_2(B^3\Pi_g) + N_2$	2.4×10^{-33}	42	
$N(2D) + M \rightarrow N + M$	2.4×10^{-14}	45	b
$N(2P) + N \rightarrow N(2D) + N$	1.8×10^{-12}	42	
$N(2P) + N_2 \rightarrow N + N_2$	2.0×10^{-18}	42	
$N_2(a'^1\Sigma_u^-) + N \rightarrow N_2 + N$	2.0×10^{-11}	46	
$N_2(a'^1\Sigma_u^-) + N_2 \rightarrow N_2 + N_2$	3.7×10^{-16}	46	
$N_2(a'^1\Sigma_u^-) + N_2 \rightarrow N_2(B^3\Pi_g) + N_2$	1.9×10^{-13}	42	
$N_2(a'^1\Sigma_u^-) + N_2(a'^1\Sigma_u^-) \rightarrow N_2^+ + N_2 + e^-$	5.0×10^{-13}	46	
$N_2(a'^1\Sigma_u^-) + N_2(a'^1\Sigma_u^-) \rightarrow N_4^+ + e^-$	1.0×10^{-11}	42	
$N_2(a'^1\Sigma_u^-) + N_2(A^3\Sigma_u^+) \rightarrow N_4^+ + e^-$	4.0×10^{-12}	42	
$N_2(A^3\Sigma_u^+) + N \rightarrow N_2 + N(2P)$	$4.0 \times 10^{-11} \times \left(\frac{300}{T_g}\right)^{0.667}$	42	
$N_2(A^3\Sigma_u^+) + N \rightarrow N_2 + N$	2.0×10^{-12}	42	
$N_2(A^3\Sigma_u^+) + N_2 \rightarrow N_2 + N_2$	3.0×10^{-16}	42	

$N_2(A^3\Sigma_u^+) + N_2\left(a'^1\Sigma_u^-\right) \rightarrow N_2^+ + N_2 + e^-$	1.0×10^{-12}	46	
$N_2(A^3\Sigma_u^+) + N_2(A^3\Sigma_u^+) \rightarrow N_2 + N_2(A^3\Sigma_u^+)$	2.0×10^{-12}	46	
$N_2(A^3\Sigma_u^+) + N_2(A^3\Sigma_u^+) \rightarrow N_2 + N_2\left(B^3\Pi_g\right)$	3.0×10^{-10}	42	
$N_2(A^3\Sigma_u^+) + N_2(A^3\Sigma_u^+) \rightarrow N_2 + N_2(C^3\Pi_u)$	1.5×10^{-10}	42	
$N_2\left(B^3\Pi_g\right) + N_2 \rightarrow N_2 + N_2$	2.0×10^{-12}	42	
$N_2\left(B^3\Pi_g\right) + N_2 \rightarrow N_2(A^3\Sigma_u^+) + N_2$	3×10^{-11}	42	
$N_2(C^3\Pi_u) + N_2 \rightarrow N_2 + \left(a'^1\Sigma_u^-\right)$	1.0×10^{-11}	42	
$O_2(g, v) + M \rightarrow O + O + M$	$\left(\frac{3.0\times10^{-6}}{T_g}\right) \times \exp\left(\frac{-59380}{T_g}\right)$		a $\alpha = 1$
$O + O + M \rightarrow O_2 + M$	$5.21 \times 10^{-35} \times \exp\left(\frac{900}{T_g}\right)$	47	b
$O + O_3 \rightarrow O_2 + O_2$	$8.0 \times 10^{-12} \times \exp\left(-\frac{2056}{T_g}\right)$	48	
$O + O_2(g, v) + M \rightarrow O_3 + M$	$1.34 \times 10^{-34} \times \left(\frac{T_g}{298}\right)^{-1.0}$	49	a, b
$O_3 + M \rightarrow O_2 + O + M$	$7.16 \times 10^{-10} \times \exp\left(-\frac{98120}{R_g T_g}\right)$	50	b, c
$O + O_2(E_x) + M \rightarrow O_3 + M$	$1.34 \times 10^{-34} \times \left(\frac{T_g}{298}\right)^{-1.0}$	49	b, d, e
$O + O_3 \rightarrow O_2 + O_2(a^1\Delta)$	$2.0 \times 10^{-11} \times \exp\left(-\frac{2280}{T_g}\right)$	42	
$O_2(a^1\Delta) + O \rightarrow O_2 + O$	7.0×10^{-16}	42	
$O_2(a^1\Delta) + O_2 \rightarrow O_2 + O_2$	$3.8 \times 10^{-18} \times \exp\left(-\frac{205}{T_g}\right)$	42	
$O_2(b^1\Sigma^+) + O \rightarrow O_2(a^1\Delta) + O$	8.1×10^{-14}	42	
$O_2(b^1\Sigma^+) + O \rightarrow O_2 + O(1D)$	$3.4 \times 10^{-11} \times \left(\frac{T_g}{300}\right)^{-0.1} \times \exp\left(-\frac{4200}{T_g}\right)$	42	
$O_2(b^1\Sigma^+) + O_2 \rightarrow O_2 + O_2(a^1\Delta)$	$4.3 \times 10^{-22} \times \left(T_g\right)^{2.4} \times \exp\left(-\frac{281}{T_g}\right)$	42	
$O_2(b^1\Sigma^+) + O_3 \rightarrow O_2 + O_2 + O$	2.2×10^{-11}	42	
$O_2(a^1\Delta) + O_3 \rightarrow O_2 + O_2 + O(1D)$	$5.2 \times 10^{-11} \times \exp\left(-\frac{2840}{T_g}\right)$	42	
$O_2(a^1\Delta) + O_2(a^1\Delta) \rightarrow O_2 + O_2(b^1\Sigma^+)$	$7.0 \times 10^{-28} \times \left(T_g\right)^{3.8} \times \exp\left(\frac{700}{T_g}\right)$	42	

$O(1D) + O \rightarrow O + O$	8.0×10^{-12}	42	
$O(1D) + O_2 \rightarrow O + O_2$	$6.4 \times 10^{-12} \times \exp\left(-\frac{67}{T_g}\right)$	42	
$O(1S) + O \rightarrow O(1D) + O(1D)$	$5.0 \times 10^{-11} \times \exp\left(-\frac{300}{T_g}\right)$	42	
$O(1S) + O_2 \rightarrow O + O_2$	$1.3 \times 10^{-12} \times \exp\left(-\frac{850}{T_g}\right)$	42	
$O(1S) + O_2 \rightarrow O + O + O$	3.0×10^{-12}	42	
$O(1S) + O_2(a^1\Delta) \rightarrow O + O + O$	3.2×10^{-11}	42	
$O(1S) + O_2(a^1\Delta) \rightarrow O(1D) + O_2(b^1\Sigma^+)$	2.9×10^{-11}	42	
$O(1S) + O_2 \rightarrow O + O_2(A^3\Sigma^+, C^3\Delta, c^1\Sigma^-)$	$3.0 \times 10^{-12} \times \exp\left(-\frac{850}{T_g}\right)$	42	f
$N + O_2(g, v) \rightarrow O + NO$	$2.36 \times 10^{-11} \times \exp\left(-\frac{44230}{R_g T_g}\right)$	51	a, c $\alpha = 0.24$
$O + N_2(g, v) \rightarrow N + NO$	$3.01 \times 10^{-10} \times \exp\left(-\frac{318000}{R_g T_g}\right)$	52	a, c $\alpha = 1$
$O_3 + N \rightarrow NO + O_2$	$5.0 \times 10^{-12} \times \exp\left(-\frac{650}{T_g}\right)$	48	
$O_3 + NO \rightarrow O_2 + NO_2$	$2.5 \times 10^{-13} \times \exp\left(-\frac{765}{T_g}\right)$	42	
$O_3 + NO_2 \rightarrow O_2 + NO_3$	$1.2 \times 10^{-13} \times \exp\left(-\frac{2450}{T_g}\right)$	41	
$NO_3 + O_3 \rightarrow NO_2 + O_2 + O_2$	1.0×10^{-17}	53	
$N + NO \rightarrow O + N_2$	1.66×10^{-11}	54	
$N + NO_2 \rightarrow O + O + N_2$	9.1×10^{-13}	42	
$N + NO_2 \rightarrow O + N_2O$	3.0×10^{-12}	42	
$N + NO_2 \rightarrow N_2 + O_2$	7.0×10^{-13}	42	
$N + NO_2 \rightarrow NO + NO$	2.3×10^{-12}	42	
$O + NO \rightarrow N + O_2$	$7.5 \times 10^{-12} \times \left(\frac{T_g}{300}\right) \times \exp\left(-\frac{19500}{T_g}\right)$	42	
$O + NO_2 \rightarrow NO + O_2$	$9.05 \times 10^{-12} \times \left(\frac{T_g}{298}\right)^{-0.52}$	55	
$O + N_2O \rightarrow NO + NO$	$1.5 \times 10^{-10} \times \exp\left(-\frac{14090}{T_g}\right)$	42	
$O + N_2O \rightarrow N_2 + O_2$	$8.3 \times 10^{-12} \times \exp\left(-\frac{14000}{T_g}\right)$	42	
$O + NO_3 \rightarrow O_2 + N_2$	1.0×10^{-11}	42	

$NO + NO \rightarrow N + NO_2$	$3.3 \times 10^{-16} \times \left(\frac{300}{T_g}\right)^{0.5} \times \exp\left(-\frac{39200}{T_g}\right)$	42	
$NO + NO \rightarrow O + N_2O$	$2.2 \times 10^{-12} \times \exp\left(-\frac{32100}{T_g}\right)$	42	
$NO + NO \rightarrow N_2 + O_2$	$5.1 \times 10^{-13} \times \exp\left(-\frac{33660}{T_g}\right)$	42	
$NO + N_2O \rightarrow N_2 + NO_2$	$4.6 \times 10^{-10} \times \exp\left(-\frac{25170}{T_g}\right)$	42	
$NO + NO_3 \rightarrow NO_2 + NO_2$	1.7×10^{-11}	42	
$NO_2 + NO_2 \rightarrow NO + NO_3$	$4.5 \times 10^{-10} \times \exp\left(-\frac{18500}{T_g}\right)$	42	
$NO_2 + NO_2 \rightarrow NO + NO + O_2$	$3.3 \times 10^{-12} \times \exp\left(-\frac{13500}{T_g}\right)$	42	
$NO_2 + NO_3 \rightarrow NO + NO_2 + O_2$	$2.3 \times 10^{-13} \times \exp\left(-\frac{1600}{T_g}\right)$	42	
$NO_3 + NO_3 \rightarrow O_2 + NO_2 + NO_2$	$4.3 \times 10^{-12} \times \exp\left(-\frac{3850}{T_g}\right)$	42	
$NO + O_2(g,v) \rightarrow O + NO_2$	$2.8 \times 10^{-12} \times \exp\left(-\frac{23400}{T_g}\right)$	42	a $\alpha = 1$
$NO + NO + O_2(g,v) \rightarrow NO_2 + NO_2$	$3.3 \times 10^{-39} \times \exp\left(-\frac{4410}{R_gT_g}\right)$	56	a, c $\alpha = 0.2$
$NO_2 + O_2(g,v) \rightarrow NO + O_3$	$2.8 \times 10^{-12} \times \exp\left(-\frac{25400}{T_g}\right)$	42	a $\alpha = 0.2$
$NO_3 + O_2(g,v) \rightarrow O_3 + NO_2$	$1.5 \times 10^{-12} \times \exp\left(-\frac{15020}{T_g}\right)$	42	a $\alpha = 0.8$
$NO + O \rightarrow NO_2$	$3.01 \times 10^{-11} \times \left(\frac{T_g}{300}\right)^{-0.75}$	57	
$NO_2 + NO + M \rightarrow N_2O_3 + M$	$3.09 \times 10^{-34} \times \left(\frac{T_g}{300}\right)^{-7.70}$	48	b
$NO_2 + NO_2 + M \rightarrow N_2O_4 + M$	$1.4 \times 10^{-33} \times \left(\frac{T_g}{300}\right)^{-3.8}$	48	b
$NO_2 + NO_3 + M \rightarrow N_2O_5 + M$	$3.7 \times 10^{-30} \times \left(\frac{300}{T_g}\right)^{4.10}$	56	b
$N + O + M \rightarrow NO + M$	$1.0 \times 10^{-32} \times \left(\frac{300}{T_g}\right)^{0.5}$	42	b
$N_2(g,v) + O + M \rightarrow N_2O + M$	$3.9 \times 10^{-35} \times \exp\left(-\frac{10400}{T_g}\right)$	42	b
$N_2O + M \rightarrow N_2 + O + M$	$1.20 \times 10^{-9} \times \exp\left(-\frac{240000}{R_gT_g}\right)$	42	b, c

$NO_2 + M \rightarrow NO + O + M$	$9.4 \times 10^{-5} \times \left(\frac{T_g}{298}\right)^{-2.66} \times \exp\left(-\frac{311000}{R_g T_g}\right)$	57	b, c
$NO_3 + M \rightarrow NO + O_2 + M$	$2.51 \times 10^{-14} \times \exp\left(-\frac{10230}{R_g T_g}\right)$	58	b, c
$NO + M \rightarrow N + O + M$	$8.7 \times 10^{-9} \times \exp\left(-\frac{75994}{T_g}\right)$	42	b
$N_2O_3 + M \rightarrow NO + NO_2 + M$	$1.91 \times 10^{-7} \times \left(\frac{T_g}{298}\right)^{-8.7} \times \exp\left(-\frac{40570}{R_g T_g}\right)$	48	b, c
$N_2O_4 + M \rightarrow NO_2 + NO_3 + M$	$1.3 \times 10^{-5} \times \left(\frac{T_g}{298}\right)^{-3.8} \times \exp\left(-\frac{53210}{R_g T_g}\right)$	48	b, c
$N_2O_5 + M \rightarrow NO_2 + NO_3 + M$	$2.1 \times 10^{-11} \times \left(\frac{300}{T_g}\right)^{-3.5} \times \exp\left(-\frac{91460}{R_g T_g}\right)$	42	b, c
$NO + O_2(g,v) + M \rightarrow NO_3 + M$	$5.65 \times 10^{-41} \times \exp\left(-\frac{1750}{R_g T_g}\right)$	59	a, b, c
$NO + O_2(E_x) + M \rightarrow NO_3 + M$	$5.65 \times 10^{-41} \times \exp\left(-\frac{1750}{R_g T_g}\right)$	59	b, d
$N + N + NO \rightarrow N_2(A^3\Sigma_u^+) + NO$	1.7×10^{-33}	42	
$N + N + NO \rightarrow N_2(B^3\Pi_g) + NO$	2.4×10^{-33}	42	
$N + N + O \rightarrow N_2(A^3\Sigma_u^+) + O$	1.0×10^{-32}	42	
$N + N + O \rightarrow N_2(B^3\Pi_g) + O$	1.4×10^{-32}	42	
$N + N + O_2 \rightarrow N_2(A^3\Sigma_u^+) + O_2$	1.7×10^{-33}	42	
$N + N + O_2 \rightarrow N_2(B^3\Pi_g) + O_2$	2.4×10^{-33}	42	
$N(2D) + N_2O \rightarrow NO + N_2$	3.5×10^{-12}	42	
$N(2D) + NO \rightarrow N_2 + O$	1.8×10^{-10}	42	
$N(2D) + O \rightarrow N + O(1D)$	4.0×10^{-13}	42	
$N(2D) + O_2(g,v) \rightarrow NO + O$	5.2×10^{-12}	42	a
$N(2P) + NO \rightarrow N_2(A^3\Sigma_u^+) + O$	3.0×10^{-11}	42	
$N(2P) + O \rightarrow N + O$	1.0×10^{-12}	42	
$N(2P) + O_2(g,v) \rightarrow NO + O$	2.6×10^{-15}	42	a
$N_2(a'^1\Sigma_u^-) + NO \rightarrow N_2 + N + O$	3.6×10^{-10}	42	
$N_2(a'^1\Sigma_u^-) + O \rightarrow NO + N$	3.0×10^{-10}	52	
$N_2(a'^1\Sigma_u^-) + O_2(g,v) \rightarrow N_2 + O + O$	2.8×10^{-11}	42	a
$N_2(A^3\Sigma_u^+) + N_2O \rightarrow N_2 + N + NO$	1.0×10^{-11}	42	

$N_2(A^3\Sigma_u^+) + NO \rightarrow N_2 + NO$	6.9×10^{-11}	42	
$N_2(A^3\Sigma_u^+) + NO_2 \rightarrow N_2 + O + NO$	1.0×10^{-12}	42	
$N_2(A^3\Sigma_u^+) + O \rightarrow N_2 + O(1S)$	2.1×10^{-11}	42	
$N_2(A^3\Sigma_u^+) + O \rightarrow NO + N(2D)$	7.0×10^{-12}	42	
$N_2(A^3\Sigma_u^+) + O_2(g,v) \rightarrow N_2 + O + O$	$2.0 \times 10^{-12} \times \left(\frac{T_g}{300}\right)^{0.55}$	42	a
$N_2(A^3\Sigma_u^+) + O_2 \rightarrow N_2 + O_2(a^1\Delta)$	$2.0 \times 10^{-13} \times \left(\frac{T_g}{300}\right)^{0.55}$	42	
$N_2(A^3\Sigma_u^+) + O_2 \rightarrow N_2 + O_2$	2.54×10^{-12}	42	
$N_2(A^3\Sigma_u^+) + O_2(g,v) \rightarrow N_2O + O$	$2.0 \times 10^{-14} \times \left(\frac{T_g}{300}\right)^{0.55}$	42	a
$N_2(B^3\Pi_g) + N_2O \rightarrow N_2 + N + NO$	0.58×10^{-10}	60	
$N_2(B^3\Pi_g) + N_2O \rightarrow N_2 + N_2 + O$	0.58×10^{-10}	60	
$N_2(B^3\Pi_g) + O \rightarrow NO + N$	3.0×10^{-10}	52	
$N_2(C^3\Pi_u) + O \rightarrow NO + N$	3.0×10^{-10}	52	
$N_2(C^3\Pi_u) + O_2(g,v) \rightarrow N_2 + O + O$	3.0×10^{-10}	42	a
$NO + O_2(E_x) \rightarrow O + NO_2$	$2.8 \times 10^{-12} \times \exp\left(-\frac{23400}{T_g}\right)$	42	d, g
$NO_3 + O_2(E_x) \rightarrow O_3 + NO_2$	$1.5 \times 10^{-12} \times \exp\left(-\frac{15020}{T_g}\right)$	42	d, h
$O(1D) + N_2 \rightarrow N_2 + O$	2.3×10^{-11}	42	
$O(1S) + N \rightarrow O + N$	1.0×10^{-12}	42	
$O(1S) + N_2(g,v) \rightarrow O + N_2(g,v)$	1.0×10^{-17}	42	
$O_2(a^1\Delta) + N \rightarrow NO + O$	$2.0 \times 10^{-14} \times \exp\left(-\frac{600}{T_g}\right)$	42	
$O_2(a^1\Delta) + N_2(g,v) \rightarrow O_2 + N_2(g,v)$	3.0×10^{-21}	42	
$O_2(a^1\Delta) + NO \rightarrow O_2 + NO$	2.5×10^{-11}	42	
$O_2(b^1\Sigma^+) + N_2 \rightarrow O_2(a^1\Delta) + N_2$	$1.7 \times 10^{-15} \times \left(\frac{T_g}{300}\right)^{1.0}$	42	
$N_2(B^3\Pi_g) + NO \rightarrow N_2(A^3\Sigma_u^+) + NO$	2.4×10^{-10}	42	
$N_2(B^3\Pi_g) + O_2(g,v) \rightarrow N_2 + O + O$	3.0×10^{-10}	42	a

[a] For any species indicated with (g,v), g and v stand for its ground and vibrationally excited state, respectively.

[b] M represents any neutral species.

[c] $R_g = 8.3144598\ J.K^{-1}.mol^{-1}$ is the universal gas constant.

[d] $O_2(E_x)$ represents the two electronically excited states: $O_2(a^1\Delta)$ and $O_2(b^1\Sigma^+)$.

[e] The rate coefficient is assumed to be equal to the rate of $O + O_2 + M \rightarrow O_3 + M$.

[f] $O_2(A^3\,\Sigma^+, C^3\,\Delta, c^1\,\Sigma^-)$ is a combination of three electronic excited states at a threshold energy of 4.5 eV.

[g] The rate coefficient is assumed to be equal to the rate of $NO + O_2 \rightarrow O + NO_2$.

[h] The rate coefficient is assumed to be equal to the rate of $NO_3 + O_2 \rightarrow O_3 + NO_2$.

Table S.10 Electron-ion recombination reactions included in the model and the corresponding rate coefficient expressions. Te is to the electron temperature in K and Tg is the gas temperature in K. The rate coefficients are expressed in $cm^3\ s^{-1}$ or $cm^6\ s^{-1}$ for binary or ternary reactions, respectively.

Reaction	Rate coefficient	Ref.	Note
$e^- + N_2^+ \rightarrow N + N(g, E_x)$	$R \times 1.8 \times 10^{-7} \times \left(\frac{300}{T_e}\right)^{0.39}$	42	a
$e^- + N_3^+ \rightarrow N_2 + N$	$2 \times 10^{-7} \times \left(\frac{300}{T_e}\right)^{0.5}$	61	
$e^- + N_3^+ \rightarrow N_2(E_x) + N$	$6.91 \times 10^{-8} \times \left(\frac{T_e}{11604.5}\right)^{-0.5}$	61	c
$e^- + N_4^+ \rightarrow N_2 + N_2$	$2.3 \times 10^{-6} \times \left(\frac{300}{T_e}\right)^{0.53}$	42	
$e^- + N_4^+ \rightarrow N_2 + N + N$	$3.13 \times 10^{-7} \times \left(\frac{T_e}{11604.5}\right)^{-0.41}$	61	
$e^- + N^+ + e^- \rightarrow e^- + N$	$7 \times 10^{-20} \times \left(\frac{300}{T_e}\right)^{4.5}$	61	
$e^- + N^+ + M \rightarrow N + M$	$6 \times 10^{-27} \times \left(\frac{300}{T_e}\right)^{1.5}$	62	b
$e^- + N_2^+ + e^- \rightarrow e^- + N_2$	$1 \times 10^{-19} \times \left(\frac{T_e}{300}\right)^{-4.5}$	61	
$e^- + N_2^+ + M \rightarrow N_2 + M$	$2.49 \times 10^{-29} \times \left(\frac{T_e}{11604.5}\right)^{-1.5}$	61	b
$e^- + O^+ + O_2 \rightarrow O + O_2$	$6 \times 10^{-27} \times \left(\frac{300}{T_e}\right)^{1.5}$	62	
$e^- + O^+ + e^- \rightarrow e^- + O$	$7 \cdot 10^{-20} \cdot \left(\frac{300}{T_e}\right)^{4.5}$	42	
$e^- + O_2^+ + M \rightarrow O_2 + M$	1×10^{-26}	36	b
$e^- + O_2^+ + e^- \rightarrow e^- + O_2$	$1 \times 10^{-19} \times \left(\frac{T_e}{300}\right)^{-4.5}$	62	
$e^- + O_2^+ \rightarrow O + O$	$6.46 \times 10^{-5} \times T_e^{-0.5} \times T_g^{-0.5}$	63	
$e^- + O_2^+ \rightarrow O + O(1D)$	$1.08 \times 10^{-7} \left(\frac{T_e}{300}\right)^{-0.7}$	42	
$e^- + O_2^+ \rightarrow O + O(1S)$	$0.14 \times 10^{-7} \left(\frac{T_e}{300}\right)^{-0.7}$	42	
$e^- + O_4^+ \rightarrow O_2 + O_2$	$1.4 \times 10^{-6} \times \left(\frac{300}{T_e}\right)^{0.5}$	42	
$e^- + NO^+ + e^- \rightarrow e^- + NO$	$1.0 \times 10^{-19} \left(\frac{T_e}{300}\right)^{-4.5}$	62	
$e^- + NO^+ + M \rightarrow NO + M$	$2.49 \times 10^{-29} \times \left(\frac{T_e}{11604.5}\right)^{-1.5}$	61	b

$e^- + NO^+ \rightarrow O + N(g, E_x)$	$R \times 4.2 \times 10^{-7} \times \left(\frac{300}{T_e}\right)^{0.85}$	42	d
$e^- + N_2O^+ \rightarrow N_2 + O$	$2.0 \times 10^{-7} \times \left(\frac{300}{T_e}\right)^{0.5}$	42	
$e^- + NO_2^+ \rightarrow NO + O$	$2.0 \times 10^{-7} \times \left(\frac{300}{T_e}\right)^{0.5}$	42	
$e^- + O_2^+N_2 \rightarrow O_2 + N_2$	$1.3 \times 10^{-6} \times \left(\frac{300}{T_e}\right)^{0.5}$	42	

[a] In $N(g, E_x)$, g stands for the ground state of atomic N and E_x represents two of its electronically excited states: $N(2D)$ and $N(2P)$; R is equal to 0.5, 0.45 and 0.05 for N, $N(2D)$ and $N(2P)$, respectively.
[b] M represents any neutral species.
[c] $N_2(E_x)$ represents $N_2(A^3\Sigma_u^+)$ and $N_2(B^3\Pi_g)$.
[d] In $N(g, E_x)$, g stands for the ground state of atomic N and E_x represents the electronic excited state $N(2D)$; R is equal to 0.2 and 0.8 for N and $N(2D)$, respectively.

Table S.11 Ion-neutral reactions included in the model and the corresponding rate coefficient expressions. T_g is the gas temperature in K. For certain reactions, T_{ion} is the effective temperature of the reacting ion in K [26]. The rate coefficients are expressed in $cm^3\ s^{-1}$ or $cm^6\ s^{-1}$ for binary or ternary reactions, respectively.

Reaction	**Rate coefficient**	**Ref.**	**Note**
$N_2^+ + N \rightarrow N^+ + N_2$	$7.2 \times 10^{-13} \times \left(\frac{T_{ion}}{300}\right)$	42	
$N_2^+ + N + N_2 \rightarrow N_3^+ + N_2$	$9.0 \times 10^{-30} \times \left(\frac{400}{T_{ion}}\right)$	42	
$N_4^+ + N_2 \rightarrow N_2^+ + N_2 + N_2$	$2.1 \times 10^{-16} \times \left(\frac{Tion}{121}\right)$	42	
$N^+ + N_2 + N_2 \rightarrow N_3^+ + N_2$	$1.7 \times 10^{-29} \times \left(\frac{300}{Tion}\right)^{2.1}$	42	
$N_2^+ + N_2 + N_2 \rightarrow N_4^+ + N_2$	$5.2 \times 10^{-29} \times \left(\frac{300}{T_{ion}}\right)^{2.2}$	42	
$N^+ + N + N_2 \rightarrow N_2^+ + N_2$	1.0×10^{-29}	42	
$N^+ + N \rightarrow N_2^+$	1.0×10^{-29}	64	
$N_3^+ + N \rightarrow N_2^+ + N_2$	6.6×10^{-11}	42	
$N_4^+ + N \rightarrow N^+ + N_2 + N_2$	1.0×10^{-11}	42	
$N_2^+ + N_2(A^3\Sigma_u^+) \rightarrow N_3^+ + N$	3.0×10^{-10}	41	
$O^- + M \rightarrow O + M + e^-$	4.0×10^{-12}	41	a
$O^- + O \rightarrow O_2 + e^-$	2.3×10^{-10}	65	
$O^- + O_2(g, v) + M \rightarrow O_3^- + M$	$1.1 \times 10^{-30} \times \exp\left(\frac{300}{T_g}\right)$	65	a, b

$O^- + O_2(g,v) \rightarrow O_3 + e^-$	5.0×10^{-15}	42	b
$O^- + O_3 \rightarrow O_2 + O_2 + e^-$	3.0×10^{-10}	66	
$O^- + O_3 \rightarrow O_3^- + O$	5.3×10^{-10}	67	
$O^+ + O + M \rightarrow O_2^+ + M$	1.0×10^{-29}	62	a
$O^+ + O_2(g,v) \rightarrow O + O_2^+$	$1.9 \times 10^{-11} \times \left(\frac{T_g}{300}\right)^{-0.5}$	68	b
$O^+ + O_3 \rightarrow O_2^+ + O_2$	1.0×10^{-10}	62	
$O_2^- + M \rightarrow O_2 + M + e^-$	$2.7 \times 10^{-10} \times \left(\frac{T_g}{300}\right)^{0.5} \times \exp\left(-\frac{5590}{T_g}\right)$	68	a
$O_2^- + O \rightarrow O_2 + O^-$	3.31×10^{-10}	65	
$O_2^- + O_2(g,v) + M \rightarrow O_4^- + M$	$3.5 \times 10^{-31} \times \left(\frac{T_g}{300}\right)^{-1.0}$	62,65,67	a, b
$O_2^- + O_2 \rightarrow O_2 + O_2 + e^-$	2.18×10^{-18}	69	
$O_2^- + O_3 \rightarrow O_3^- + O_2$	4.0×10^{-10}	65	
$O_2^+ + O_2(g,v) + M \rightarrow O_4^+ + M$	$2.4 \times 10^{-30} \times \left(\frac{T_g}{300}\right)^{-3.2}$	62	a, b
$O_3^- + M \rightarrow O_3 + M + e^-$	2.3×10^{-11}	68	a
$O_3^- + O \rightarrow O_2 + O_2 + e^-$	1.0×10^{-13}	67	
$O_3^- + O \rightarrow O_2^- + O_2$	2.5×10^{-10}	35	
$O_3^- + O \rightarrow O_3 + O^-$	1.0×10^{-13}	65	
$O_3^- + O_3 \rightarrow O_2 + O_2 + O_2 + e^-$	3.0×10^{-10}	67	
$O_4^- + O \rightarrow O^- + O_2 + O_2$	3.0×10^{-10}	62	
$O_4^- + O \rightarrow O_3^- + O_2$	4.0×10^{-10}	62	
$O_4^- + O_2 \rightarrow O_2^- + O_2 + O_2$	$1.0 \times 10^{-10} \times \exp\left(-\frac{1044}{T_g}\right)$	42	
$O_4^+ + O \rightarrow O_2^+ + O_3$	3.0×10^{-10}	62	
$O_4^+ + O_2 \rightarrow O_2^+ + O_2 + O_2$	$3.3 \times 10^{-6} \times \left(\frac{300}{T_g}\right)^{4.0} \times \exp\left(-\frac{5030}{T_g}\right)$	62	
$O^- + O_2(a^1\Delta) \rightarrow O_3 + e^-$	3.0×10^{-10}	42	
$O_2^- + O_2(a^1\Delta) \rightarrow O_2 + O_2 + e^-$	2.0×10^{-10}	42	
$O_2^- + O_2(b^1\Sigma^+) \rightarrow O_2 + O_2 + e^-$	3.6×10^{-10}	42	
$O_2^+ + O_2(E_x) + M \rightarrow O_4^+ + M$	$2.4 \times 10^{-30} \times \left(\frac{T_g}{300}\right)^{-3.2}$	42	a, c, d
$O_4^+ + O_2(a^1\Delta) \rightarrow O_2^+ + O_2 + O_2$	1.0×10^{-10}	42	
$O_4^- + O_2(E_x) \rightarrow O_2^- + O_2 + O_2$	1.0×10^{-10}	42	c
$O^- + O_2(a^1\Delta) \rightarrow O_2^- + O$	1.0×10^{-10}	42	

$O^- + O_2(E_x) + M \rightarrow O_3^- + M$	$1.1 \times 10^{-30} \times \exp\left(\frac{300}{T_g}\right)$	42	a, c, e
$O_2^- + O_2(E_x) + M \rightarrow O_4^- + M$	$3.5 \times 10^{-31} \times \exp\left(\frac{T_g}{300}\right)^{-1.0}$	62	a, c, f
$N^+ + N + O_2 \rightarrow N_2^+ + O_2$	1.0×10^{-29}	42	
$N^+ + N_2O \rightarrow NO^+ + N_2$	5.5×10^{-10}	42	
$N^+ + NO \rightarrow N_2^+ + O$	3.0×10^{-12}	42	
$N^+ + NO \rightarrow NO^+ + N$	8.0×10^{-10}	42	
$N^+ + NO \rightarrow O^+ + N_2$	1.0×10^{-12}	42	
$N^+ + O + M \rightarrow NO^+ + M$	1.0×10^{-29}	42	a
$N^+ + O \rightarrow N + O^+$	1.0×10^{-12}	42	
$N^+ + O_2 \rightarrow NO^+ + O$	2.5×10^{-10}	42	
$N^+ + O_2 \rightarrow O^+ + NO$	2.8×10^{-11}	42	
$N^+ + O_2 \rightarrow O_2^+ + N$	2.8×10^{-10}	42	
$N^+ + O_3 \rightarrow NO^+ + O_2$	5.0×10^{-10}	42	
$N_2^+ + N_2O \rightarrow N_2O^+ + N_2$	5.0×10^{-10}	42	
$N_2^+ + N_2O \rightarrow NO^+ + N + N_2$	4.0×10^{-10}	42	
$N_2^+ + NO \rightarrow NO^+ + N_2$	3.3×10^{-10}	42	
$N_2^+ + O \rightarrow NO^+ + N$	$1.3 \times 10^{-10} \times \left(\frac{300}{T_{ion}}\right)^{0.5}$	42	
$N_2^+ + O_2 \rightarrow O_2^+ + N_2$	$6.0 \times 10^{-11} \times \left(\frac{300}{T_{ion}}\right)^{0.5}$	42	
$N_2^+ + O_3 \rightarrow O_2^+ + O + N_2$	1.0×10^{-10}	42	
$N_2O^- + N \rightarrow NO + N_2 + e^-$	5.0×10^{-10}	41	
$N_2O^- + O \rightarrow NO + NO + e^-$	1.5×10^{-10}	41	
$N_2O^+ + NO \rightarrow NO^+ + N_2O$	2.9×10^{-10}	42	
$N_3^+ + NO \rightarrow N_2O^+ + N_2$	7.0×10^{-11}	42	
$N_3^+ + NO \rightarrow NO^+ + N + N_2$	7.0×10^{-11}	42	
$N_3^+ + O_2 \rightarrow NO_2^+ + N_2$	4.4×10^{-11}	42	
$N_3^+ + O_2 \rightarrow O_2^+ + N + N_2$	2.3×10^{-11}	42	
$N_4^+ + NO \rightarrow NO^+ + N_2 + N_2$	4.0×10^{-10}	42	
$N_4^+ + O \rightarrow O^+ + N_2 + N_2$	2.5×10^{-10}	42	
$N_4^+ + O_2 \rightarrow O_2^+ + N_2 + N_2$	2.5×10^{-10}	42	
$NO^- + N_2O \rightarrow NO + N_2O + e^-$	$4.26 \times 10^{-10} \times \exp\left(-\frac{107.2}{T_g}\right)$	70	
$NO^- + NO \rightarrow NO + NO + e^-$	$3.28 \times 10^{-10} \times \exp\left(-\frac{105.1}{T_g}\right)$	70	
$NO^- + N \rightarrow N_2O + e^-$	5.0×10^{-10}	42	
$NO^- + N_2O \rightarrow NO_2^- + N_2$	2.8×10^{-14}	42	

$NO^- + NO_2 \rightarrow NO_2^- + NO$	7.4×10^{-10}	42	
$NO^- + O \rightarrow NO_2 + e^-$	1.5×10^{-10}	41	
$NO^- + O_2 \rightarrow O_2^- + NO$	5.0×10^{-10}	42	
$NO_2^- + N \rightarrow NO + NO + e^-$	5.0×10^{-10}	41	
$NO_2^- + N_2O_5 \rightarrow NO_3^- + NO_2 + NO_2$	7.0×10^{-10}	42	
$NO_2^- + NO_2 \rightarrow NO_3^- + NO$	4.0×10^{-12}	42	
$NO_2^- + NO_3 \rightarrow NO_3^- + NO_2$	5.0×10^{-10}	42	
$NO_2^- + O_3 \rightarrow NO_3^- + O_2$	1.8×10^{-11}	42	
$NO_2^+ + NO \rightarrow NO^+ + NO_2$	2.9×10^{-10}	42	
$NO_3^- + N \rightarrow NO + NO_2 + e^-$	5.0×10^{-10}	41	
$NO_3^- + NO \rightarrow NO_2^- + NO_2$	3.0×10^{-15}	42	
$NO_3^- + O \rightarrow NO + O_3 + e^-$	1.5×10^{-10}	41	
$O^- + N \rightarrow NO + e^-$	2.6×10^{-10}	42	
$O^- + N_2(g,v) \rightarrow N_2O + e^-$	0.5×10^{-13}	42	b
$O^- + N_2(A^3\Sigma_u^+) \rightarrow O + N_2 + e^-$	2.2×10^{-9}	42	
$O^- + N_2(B^3\Pi_g) \rightarrow O + N_2 + e^-$	1.9×10^{-9}	42	
$O^- + N_2O \rightarrow N_2O^- + O$	2.0×10^{-12}	42	
$O^- + N_2O \rightarrow NO^- + NO$	2.0×10^{-10}	42	
$O^- + NO + M \rightarrow NO_2^- + M$	1.0×10^{-29}	42	a
$O^- + NO \rightarrow NO_2 + e^-$	2.6×10^{-10}	42	
$O^- + NO_2 \rightarrow NO_2^- + O$	1.2×10^{-9}	42	
$O^+ + N + M \rightarrow NO^+ + M$	1.0×10^{-29}	42	a
$O^+ + N \rightarrow N^+ + O$	1.3×10^{-10}	42	
$O^+ + N_2(g,v) + M \rightarrow NO^+ + N + M$	$6.0 \times 10^{-29} \times \left(\frac{300}{T_{ion}}\right)^2$	42	a, b
$O^+ + N_2(g,v) \rightarrow NO^+ + N$	$(1.5 - 2.0 \times 10^{-3} \times T_{ion} + 9.6 \times 10^{-7} \times T_{ion}^2) \times 1.0 \times 10^{-12}$	42	b
$O^+ + N_2O \rightarrow N_2O^+ + O$	2.2×10^{-10}	42	
$O^+ + N_2O \rightarrow NO^+ + NO$	2.3×10^{-10}	42	
$O^+ + N_2O \rightarrow O_2^+ + N_2$	2.0×10^{-11}	42	
$O^+ + NO \rightarrow NO^+ + O$	2.4×10^{-11}	42	
$O^+ + NO \rightarrow O_2^+ + N$	3.0×10^{-12}	42	
$O^+ + NO_2 \rightarrow NO_2^+ + O$	1.6×10^{-9}	42	
$O_2^- + N \rightarrow NO_2 + e^-$	5.0×10^{-10}	42	
$O_2^- + N_2(B^3\Pi_g) \rightarrow O_2 + N_2 + e^-$	2.5×10^{-9}	42	
$O_2^- + N_2(A^3\Sigma_u^+) \rightarrow O_2 + N_2 + e^-$	2.1×10^{-9}	42	
$O_3^- + N_2(B^3\Pi_g) \rightarrow O_3 + N_2 + e^-$	2.5×10^{-9}	41	

$O_3^- + N_2(A^3\Sigma_u^+) \rightarrow O_3 + N_2 + e^-$	2.1×10^{-9}	41	
$NO^- + N_2(B^3\Pi_g) \rightarrow NO + N_2 + e^-$	2.5×10^{-9}	41	
$NO^- + N_2(A^3\Sigma_u^+) \rightarrow NO + N_2 + e^-$	2.1×10^{-9}	41	
$N_2O^- + N_2(B^3\Pi_g) \rightarrow N_2O + N_2 + e^-$	2.5×10^{-9}	41	
$N_2O^- + N_2(A^3\Sigma_u^+) \rightarrow N_2O + N_2 + e^-$	2.1×10^{-9}	41	
$NO_2^- + N_2(B^3\Pi_g) \rightarrow NO_2 + N_2 + e^-$	2.5×10^{-9}	41	
$NO_2^- + N_2(A^3\Sigma_u^+) \rightarrow NO_2 + N_2 + e^-$	2.1×10^{-9}	41	
$NO_3^- + N_2(B^3\Pi_g) \rightarrow NO_3 + N_2 + e^-$	2.5×10^{-9}	41	
$NO_3^- + N_2(A^3\Sigma_u^+) \rightarrow NO_3 + N_2 + e^-$	2.1×10^{-9}	41	
$O_2^- + NO_2 \rightarrow NO_2^- + O_2$	7.0×10^{-10}	42	
$O_2^- + NO_3 \rightarrow NO_3^- + O_2$	5.0×10^{-10}	42	
$O_2^+ + N \rightarrow NO^+ + O$	1.2×10^{-10}	42	
$O_2^+ + N_2(g,v) + N_2 \rightarrow O_2^+N_2 + N_2$	$9.0 \times 10^{-31} \times \left(\frac{300}{T_{ion}}\right)^2$	42	b
$O_2^+ + N_2(g,v) \rightarrow NO^+ + NO$	1.0×10^{-17}	42	b
$O_2^+ + NO \rightarrow NO^+ + O_2$	6.3×10^{-10}	42	
$O_2^+ + NO_2 \rightarrow NO^+ + O_3$	1.0×10^{-11}	42	
$O_2^+ + NO_2 \rightarrow NO_2^+ + O_2$	6.6×10^{-10}	42	
$O_2^+N_2 + N_2 \rightarrow O_2^+ + N_2 + N_2$	$1.1 \times 10^{-6} \times \left(\frac{300}{T_{ion}}\right)^{5.3} \times \exp\left(-\frac{2360}{T_{ion}}\right)$	42	
$O_2^+N_2 + O_2 \rightarrow O_4^+ + N_2$	1.0×10^{-9}	42	
$O_3^- + N \rightarrow NO + O_2 + e^-$	5.0×10^{-10}	41	
$O_3^- + NO \rightarrow NO_2^- + O_2$	2.6×10^{-12}	42	
$O_3^- + NO \rightarrow NO_3^- + O$	1.0×10^{-11}	42	
$O_3^- + NO_2 \rightarrow NO_2^- + O_3$	7.0×10^{-11}	42	
$O_3^- + NO_2 \rightarrow NO_3^- + O_2$	2.0×10^{-11}	42	
$O_3^- + NO_3 \rightarrow NO_3^- + O_3$	5.0×10^{-10}	42	
$O_4^- + N_2 \rightarrow O_2^- + O_2 + N_2$	$1 \times 10^{-10} \times \exp\left(-\frac{1044}{T_g}\right)$	42	

$O_4^- + NO \rightarrow NO_3^- + O_2$	2.5×10^{-10}	42	
$O_4^+ + N_2(g,v) \rightarrow O_2^+N_2 + O_2$	$4.6 \times 10^{-12} \times \left(\frac{T_{ion}}{300}\right)^{2.5} \times \exp\left(-\frac{2650}{T_{ion}}\right)$	42	b
$O_4^+ + NO \rightarrow NO^+ + O_2 + O_2$	1.0×10^{-10}	42	

[a] M represents any neutral species.
[b] For any species indicated with (g,v), g and v stand for its ground and vibrationally excited state, respectively.
[c] $O_2(E_x)$ represents the electronically excited states: $O_2(a^1\Delta)$and $O_2(b^1\Sigma^+)$.
[d] The rate coefficient is assumed to be equal to the rate of $O_2^+ + O_2 + M \rightarrow O_4^+ + M$.
[e] The rate coefficient is assumed to be equal to the rate of $O^- + O_2 + M \rightarrow O_3^- + M$.
[f] The rate coefficient is assumed to be equal to the rate of $O_2^- + O_2 + M \rightarrow O_4^- + M$.

Table S.12 Ion-ion reactions included in the model, the corresponding rate coefficient expressions and the references. T_g is the gas temperature in K. The rate coefficients are expressed in $cm^3\ s^{-1}$or $cm^6\ s^{-1}$ for binary or ternary reactions, respectively.

Reaction	**Rate coefficient**	**Ref.**	**Note**
$O^- + O^+ + M \rightarrow O_2 + M$	$1.0 \times 10^{-25} \times \left(\frac{300}{T_g}\right)^{2.5}$	68	a
$O^- + O_2^+ + M \rightarrow O_3 + M$	$1.0 \times 10^{-25} \times \left(\frac{300}{T_g}\right)^{2.5}$	68	a
$O_2^- + O^+ + M \rightarrow O_3 + M$	$1.0 \times 10^{-25} \times \left(\frac{300}{T_g}\right)^{2.5}$	68	a
$O_2^- + O_2^+ + M \rightarrow O_2 + O_2 + M$	$1.0 \times 10^{-25} \times \left(\frac{300}{T_g}\right)^{2.5}$	68	a
$O_3^- + O^+ + M \rightarrow O_3 + O + M$	$2.0 \times 10^{-25} \times \left(\frac{300}{T_g}\right)^{2.5}$	41	a
$O_3^- + O_2^+ + M \rightarrow O_3 + O_2 + M$	$2.0 \times 10^{-25} \times \left(\frac{300}{T_g}\right)^{2.5}$	41	a
$O^- + O_2^+ \rightarrow O + O + O$	$2.60 \times 10^{-8} \times \left(\frac{300}{T_g}\right)^{0.44}$	65	a
$O_3^- + O_2^+ \rightarrow O + O + O_3$	$1.0 \times 10^{-7} \times \left(\frac{300}{T_g}\right)^{0.5}$	65	a

$O^- + O^+ \rightarrow O + O$	$4.0 \times 10^{-8} \times \left(\frac{300}{T_g}\right)^{0.43}$	65	
$O^- + O_2^+ \rightarrow O_2 + O$	$2.6 \times 10^{-8} \times \left(\frac{300}{T_g}\right)^{0.44}$	65	
$O_2^- + O^+ \rightarrow O + O_2$	$2.7 \times 10^{-7} \times \left(\frac{300}{T_g}\right)^{0.5}$	65	
$O_2^- + O_2^+ \rightarrow O_2 + O_2$	$2.01 \times 10^{-7} \times \left(\frac{300}{T_g}\right)^{0.5}$	65	
$O_2^- + O_2^+ \rightarrow O_2 + O + O$	$1.01 \times 10^{-13} \times \left(\frac{300}{T_g}\right)^{0.5}$	65	
$O_3^- + O^+ \rightarrow O_3 + O$	$1.0 \times 10^{-7} \times \left(\frac{300}{T_g}\right)^{0.5}$	69	
$O_3^- + O_2^+ \rightarrow O_2 + O_3$	$2.0 \times 10^{-7} \times \left(\frac{300}{T_g}\right)^{0.5}$	65	
$NO^- + A^+ + M \rightarrow NO + A + M$	$2.0 \times 10^{-25} \times \left(\frac{300}{T_g}\right)^{2.5}$	41	a, b
$NO_2^- + A^+ + M \rightarrow NO_2 + A + M$	$2.0 \times 10^{-25} \times \left(\frac{300}{T_g}\right)^{2.5}$	41	a, b
$N_2O^- + A^+ + M \rightarrow N_2O + A + M$	$2.0 \times 10^{-25} \times \left(\frac{300}{T_g}\right)^{2.5}$	41	a, b
$NO_3^- + A^+ + M \rightarrow NO_3 + A + M$	$2.0 \times 10^{-25} \times \left(\frac{300}{T_g}\right)^{2.5}$	41	a, b
$O_3^- + B^+ + M \rightarrow O_3 + B + M$	$2.0 \times 10^{-25} \times \left(\frac{300}{T_g}\right)^{2.5}$	41	a, c

[a] M represents any neutral species.
[b] A represents N, O, N_2, O_2, NO, NO_2 and N_2O species.
[c] B represents N, N_2, NO, NO_2 and N_2O species.

Table S.13 Optical transitions of N_2 and O_2 species. The rate coefficients are expressed in s^{-1}.

Reaction	**Rate coefficient**	**Ref.**	**Note**
$N_2(A^3\Sigma_u^+) \rightarrow N_2$	0.5	42	
$N_2(B^3\Pi_g) \rightarrow N_2(A^3\Sigma_u^+)$	1.35×10^5	42	
$N_2(a'^1\Sigma_u^-) \rightarrow N_2$	1.0×10^2	42	
$N_2(C^3\Pi_u) \rightarrow N_2(B^3\Pi_g)$	2.45×10^7	42	
$O_2(a^1\Delta) \rightarrow O_2$	2.6×10^{-4}	42	
$O_2(b^1\Sigma^+) \rightarrow O_2$	8.5×10^{-2}	42	
$O_2(b^1\Sigma^+) \rightarrow O_2(a^1\Delta)$	1.5×10^{-3}	42	

$O_2(A^3\Sigma^+, C^3\Delta, c^1\Sigma^-) \rightarrow O_2$	11	[42]	a

[a] $O_2(A^3\Sigma^+, C^3\Delta, c^1\Sigma^-)$ is a combination of three electronic excited states at a threshold energy of 4.5 eV.

The reaction rate expressions of the VT relaxations and VV exchanges between N_2 - N_2, N_2 - O_2 and O_2 - O_2 are calculated using the Forced Harmonic Oscillator (FHO) model proposed by Adamovich et al.[71] This method offers a semi-classical non-perturbative analytical solution for VT and VV transitions of diatomic molecules by averaging the VT and VV probabilities (P_{VT} and P_{VV}) over the one-dimensional Boltzmann distribution.

$$P_{VT}(i \rightarrow f) = \frac{(n_s)^s}{(s!)^2} \cdot \varepsilon^s \cdot \exp\left(-\frac{2n_s}{s+1}\varepsilon\right) \tag{10}$$

$$P_{VV}(i_1, i_2 \rightarrow f_1, f_2) \cong \frac{\left[n_s^{(1)} n_s^{(2)}\right]^s}{(s!)^2} \cdot \left(\frac{\rho_\varepsilon^2}{4}\right)^s \cdot \exp\left[-\frac{2n_s^{(1)} n_s^{(2)}}{s+1}\frac{\rho_\varepsilon^2}{4}\right] \tag{11}$$

with $s = |i - f|$, $n_s = \left[\frac{\max(i,f)!}{\min(i,f)!}\right]^{1/s}$. ρ_ε and ε are collision and potential specific parameters.

Table S. 14 Vibrational – vibrational exchanges and vibrational – translational relaxations for N_2 (as an example) and the rate coefficient expression..

Reaction	**Rate coefficient**
$N_2(v_i) + M \rightarrow N_2(v_i - 1) + M$	$Z \cdot \left(\frac{m}{kT}\right) \int_0^\infty P_{VT}(\bar{v}) \cdot \exp\left(\frac{-mv^2}{2kT}\right) vdv$
$N_2(v_i) + N_2(v_j) \rightarrow N_2(v_i - 1) + N_2(v_j + 1)$	$Z \cdot \left(\frac{m}{kT}\right) \int_0^\infty P_{VV}(\bar{v}) \cdot \exp\left(\frac{-mv^2}{2kT}\right) vdv$
M represents any neutral particle in the plasma. v_i and v_j are the vibrational levels of N_2 (0-24). Z is the collision frequency and v is the particle velocity.	

The reaction rates of the VT relaxations between N_2 – N are based on quasi classical calculations that have been reproduced through a fit as proposed by Esposito et al.[72], for the following general reaction:

$N_2(v) + N \rightarrow N_2(w) + N$, with $v > w$

All the relevant trends in the rate were taken into consideration by using an additive model into the exponential argument of the reaction rate constant, as shown in the following expression (valid for $v = 1 - 66$ and $\Delta v = 1 - 30$):

$$K(v,T,\Delta v) = \exp\left(a_1(v,\Delta v) + \frac{a_2(v,\Delta v)}{T} + \frac{a_3(v,\Delta v)}{T^2} + \frac{a_4(v,\Delta v)}{T^3} + a_5(v,\Delta v)\cdot \ln(T)\right) \quad (12)$$

where

$$a_i(v,\Delta v) = z_{i0}(\Delta v) + z_{i1}(\Delta v)v + z_{i2}(\Delta v)v^2 + z_{i3}(\Delta v)v^3 + z_{i4}(\Delta v)v^4 \quad (13)$$

$$z_{ij}(\Delta v) = b_{ij} + c_{ij}\Delta v \quad (14)$$

For which the parameters are reported in [72].

Similarly, the reaction rates of the VT relaxations between O_2 – O are based on quasi classical calculations that have been reproduced through a fit as proposed by Esposito et al.[73], for the following general reaction:

$O_2(v) + O \rightarrow O_2(w) + O$, with $v > w$

The reaction rate constant is then determined based on the following expression:

$$K(T,v,\Delta v) = DegF \cdot \exp(a_1(v,\Delta v) + \frac{a_2(v,\Delta v)}{\ln(T)} + a_3(v,\Delta v)\cdot \ln(T) \quad (15)$$

where Δv is $(v - w)$

$$a_i(v,\Delta v) = b_{i1}(\Delta v) + b_{i2}(\Delta v)\cdot \ln(v) + \frac{b_{i3}(\Delta v) + b_{i4}(\Delta v)v + b_{i5}(\Delta v)v^2}{10^{21} + \exp(v)} \quad (15)$$

$$b_{ij}(\Delta v) = c_{ij1} + c_{ij2}\cdot \ln(\Delta v) + c_{ij3}\cdot \Delta v \cdot \exp(-\Delta v) + c_{ij4}\cdot \Delta v \cdot \Delta v \quad (16)$$

The coefficients c_{ijk} have been generated using a linear least squares method and are reported in[73] where the degenary factor (DegF) is also explained.

4 References

(1) Pei, X.; Gidon, D.; Yang, Y. J.; Xiong, Z.; Graves, D. B. Reducing Energy Cost of NO x Production in Air Plasmas. *Chem. Eng. J.* **2019**, *362* (x), 217–228. DOI:10.1016/j.cej.2019.01.011.

(2) Birkeland, K. On the Oxidation of Atmospheric Nitrogen in Electric Arcs. *Trans. Faraday. Soc.* **1906**, *58*, 98–116. DOI:https://doi.org/10.1039/TF9060200098.

(3) Partridge, W. S.; Parlin, R. B.; Zwolinski, B. J. Fixation of Nitrogen in a Crossed Discharge. *Ind. Eng. Chem.* **1954**, *46*, 1468−1471. DOI:10.1021/ie50535a044.

(4) Mutel, B.; Dessaux, O.; Goudmand, P. Energy Cost Improvement Ofthe Nitrogen Oxides Synthesis in a Low Pressure Plasma. *Rev. Phys. Appl.* **1984**, *19*, 461–464. DOI:10.1051/rphysap:01984001906046100.

(5) Polak, L. S.; Ovsiannikov, A. A.; Slovetsky, D. I.; Vurzel, F. B. *Theoretical and Applied Plasma Chemistry*; Nauka (Science): Moscow, 1975.

(6) Asisov, R. I.; Givotov, V. K.; Rusanov, V. D.; Fridman, A. No Title. *Sov. Phys. High Energy Chem (Khimia Vysok. Energ.* **1980**, *14*, 366.

(7) Patil, B. S.; Cherkasov, N.; Lang, J.; Ibhadon, A. O.; Hessel, V.; Wang, Q. Low Temperature Plasma-Catalytic NOxsynthesis in a Packed DBD Reactor: Effect of Support Materials and Supported Active Metal Oxides. *Appl. Catal. B Environ.* **2016**, *194* (2), 123–133. DOI:10.1016/j.apcatb.2016.04.055.

(8) Malik, M. A.; Jiang, C.; Heller, R.; Lane, J.; Hughes, D.; Schoenbach, K. H. Ozone-Free Nitric Oxide Production Using an Atmospheric Pressure Surface Discharge - a Way to Minimize Nitrogen Dioxide Co-Production. *Chem. Eng. J.* **2016**, *283*, 631–638. DOI:10.1016/j.cej.2015.07.092.

(9) Patil, B. S.; Rovira Palau, J.; Hessel, V.; Lang, J.; Wang, Q. Plasma Nitrogen Oxides Synthesis in a Milli-Scale Gliding Arc Reactor: Investigating the Electrical and Process Parameters. *Plasma Chem. Plasma Process.* **2016**, *36* (1), 241–257. DOI:10.1007/s11090-015-9671-4.

(10) Reuvers, J. G. Brightling, J. R. Sheldon, D. Ammonia Technology Development from Haber-Bosch to Current Times. *Conf. Int. Fertil. Soc.* **2013**, *4* (May), 1–33. DOI:10.1039/C9EE02873K.

(11) S. Pancheshnyi, B. Eismann, G.J.M. Hagelaar, L. C. P. Computer code ZDPlaskin http://www.zdplaskin.laplace.univ-tlse.fr.

(12) Hagelaar, G. J. M.; Pitchford, L. C. Solving the Boltzmann Equation to Obtain Electron Transport Coefficients and Rate Coefficients for Fluid Models. *Plasma Sources Sci. Technol.* **2005**, *14*, 722–733. DOI:10.1088/0963-0252/14/4/011.

(13) Lieberman, M. A.; Lichtenberg, A. J. *Principles of Plasma Discharges and Materials Processing: Second Edition*, 2nd Editio.; Wiley-Interscience, 2005. DOI:10.1002/0471724254.

(14) Trenchev, G.; Kolev, S.; Bogaerts, A. A 3D Model of a Reverse Vortex Flow Gliding Arc Reactor. *Plasma Sources Sci. Technol.* **2016**, *25* (3), 035014–035026. DOI:10.1088/0963-0252/25/3/035014.

(15) Trenchev, G.; Kolev, S.; Wang, W.; Ramakers, M.; Bogaerts, A. CO_2 Conversion in a Gliding Arc Plasmatron: Multidimensional Modeling for Improved Efficiency. *J. Phys. Chem. C* **2017**, *121* (44), 24470–24479. DOI:10.1021/acs.jpcc.7b08511.

(16) Bogaerts, A. Kozák, T. van Laer, K. Snoeckx, R. Plasma-Based Conversion of CO2: Current Status and Future Challenges. *Faraday Discuss.* **2015**, *183*, 217–232. DOI:10.1039/c5fd00053j.
(17) Kozák, T.; Bogaerts, A. Splitting of CO 2 by Vibrational Excitation in Non-Equilibrium Plasmas: A Reaction Kinetics Model. *Plasma Sources Sci. Technol.* **2014**, *23* (4), 045004–045021. DOI:10.1088/0963-0252/23/4/045004.
(18) Ramakers, M.; Trenchev, G.; Heijkers, S.; Wang, W.; Bogaerts, A. Gliding Arc Plasmatron: Providing an Alternative Method for Carbon Dioxide Conversion. *ChemSusChem* **2017**, *10* (12), 2642–2652. DOI:10.1002/cssc.201700589.
(19) Cleiren, E.; Heijkers, S.; Ramakers, M.; Bogaerts, A. Dry Reforming of Methane in a Gliding Arc Plasmatron: Towards a Better Understanding of the Plasma Chemistry. *ChemSusChem* **2017**, *10* (20), 4025–4036. DOI:10.1002/cssc.201701274.
(20) Heijkers, S.; Bogaerts, A. CO2Conversion in a Gliding Arc Plasmatron: Elucidating the Chemistry through Kinetic Modeling. *J. Phys. Chem. C* **2017**, *121* (41), 22644–22655. DOI:10.1021/acs.jpcc.7b06524.
(21) Gröger, S.; Hamme, M.; Bibinov, N.; Awakowicz, P.; Ramakers, M.; Bogaerts, A.; Medrano, J. A.; Gallucci, F. Characterization of a Nitrogen Gliding Arc Plasmatron Using Optical Emission Spectroscopy and High-Speed Camera. *J. Phys. D. Appl. Phys.* **2019**, *52* (6), 065201–065213. DOI:10.1088/1361-6463/aaefe4.
(22) Fridman, A. *Plasma Chemistry*; Intergovernmental Panel on Climate Change, Ed.; Cambridge University Press: Cambridge, 2005. DOI:10.1017/CBO9781107415324.004.
(23) Heijkers, S.; Snoeckx, R.; Kozák, T.; Silva, T.; Godfroid, T.; Britun, N.; Snyders, R.; Bogaerts, A. CO<inf>2</Inf> Conversion in a Microwave Plasma Reactor in the Presence of N<inf>2</Inf>: Elucidating the Role of Vibrational Levels. *J. Phys. Chem. C* **2015**, *119* (23), 12815–12828. DOI:10.1021/acs.jpcc.5b01466.
(24) Wang, W.; Patil, B.; Heijkers, S.; Hessel, V.; Bogaerts, A. Nitrogen Fixation by Gliding Arc Plasma: Better Insight by Chemical Kinetics Modelling. *ChemSusChem* **2017**, *10* (10), 2110–2157. DOI:10.1002/cssc.201700611.
(25) Pei, X.; Gidon, D.; Yang, Y. J.; Xiong, Z.; Graves, D. B. Reducing Energy Cost of NO x Production in Air Plasmas. *Chem. Eng. J.* **2019**, *362* (x), 217–228. DOI:10.1016/j.cej.2019.01.011.
(26) Laporta, V.; Little, D. A.; Celiberto, R.; Tennyson, J. Electron-Impact Resonant Vibrational Excitation and Dissociation Processes Involving Vibrationally Excited N2molecules. *Plasma Sources Sci. Technol.* **2014**, *23*, 065002. DOI:10.1088/0963-0252/23/6/065002.
(27) Alves, L. L. "The IST-Lisbon Database on LXCat." *J. phys. Conf. Ser.* **2014**, *565* (1).
(28) Morgan database, www.lxcat.net, retrieved in february 2018.
(29) Phelps, A. V.; Pitchford, L. C. Anisotropic Scattering of Electrons by N2 and Its Effect on Electron Transport. *Phys. Rev.* **1985**, *31*, 2932–2949. DOI:10.1103/PhysRevA.31.2932.
(30) Laporta, V.; Celliberto, R.; Tennyson, J. Resonant Vibrational-Excitation Cross Sections and Rate Constants for Low-Energy Electron Scattering by Molecular Oxygen. *plasma sources sci. Technol.* **2013**, *22*, 025001. DOI:10.1088/0963-0252/22/2/025001.
(31) Itikawa, Y. Cross Sections for Electron Collisions with Oxygen Molecules. *J. Phys. Chem. Ref. Data* **2009**, *38* (1), 1–20. DOI:10.1063/1.3025886.
(32) Itikawa, Y. Cross Sections for Electron Collisions with Oxygen Molecules. *J. Phys. Chem. Ref. Data* **2009**, *38* (1), 1–20. DOI:10.1063/1.3025886.

(33) Eliasson, B.; Kogelschatz, U. *Basic Data for Modelling of Electrical Discharges in Gases: Oxygen*; Baden: ABB Asea Brown Boveri, 1986.
(34) Lawton, S. A.; Phelps, A. V. Excitation of the B^1 Sigma_g^+ State of O_2 by Low Energy Electrons. *J. chem. Phys.* **1978**, *69* (3), 1055–1068. DOI:10.1063/1.436700.
(35) Khvorostovskaya, L. E.; Yankovsky, V. A. Negative Ions, Ozone, and Metastable Components in Dc Oxygen Glow Discharge. *Contrib. to Plasma Phys.* **1991**, *31* (1), 71–88. DOI:10.1002/ctpp.2150310109.
(36) Hokazono, H.; Obara, M.; Midorikawa, K.; Tashiro, H. Theoretical Operational Life Study of the Closed-Cycle Transversely Excited Atmospheric CO2laser. *J. Appl. Phys.* **1991**, *69* (10), 6850–6868. DOI:10.1063/1.347675.
(37) Itikawa database, www.lxcat.net, retrieved in february 2018.
(38) Quantemol database, www.lxcat.net, retrieved in february 2018.
(39) Hayashi database, www.lxcat.net, retrieved in february 2018.
(40) Gordillo-V'azquez, F. J. Air Plasma Kinetics under the Influence of Sprites. *J. Phys. D. Appl. Phys.* **2008**, *41*, 234016–234049. DOI:10.1088/0022-3727/41/23/234016.
(41) Wang, W.; Snoeckx, R.; Zhang, X.; Cha, M. S.; Bogaerts, A. Modeling Plasma-Based CO2 and CH4 Conversion in Mixtures with N2, O2, and H2O: The Bigger Plasma Chemistry Picture. *J. Phys. Chem. C* **2018**, *122* (16), 8704–8723. DOI:10.1021/acs.jpcc.7b10619.
(42) Capitelli. *Plasma Kinetics in Atmospheric Gases*; Springer, 2000.
(43) Kewley, D. J.; Hornung, H. G. Free-Piston Shock-Tube Study of Nitrogen Dissociation. *Chem. Phys. Lett.* **1974**, *25* (4), 531–536. DOI:10.1016/0009-2614(74)85360-1.
(44) Clyne, M. A. A. .; Stedman, D. H. Rate of Recombination of Nitrogen Atoms. *J. Phys. Chem.* **1967**, *71* (9), 3071–3073. DOI:10.1021/j100868a056.
(45) Van Gaens, W.; Bogaerts, A. Erratum: Kinetic Modelling for an Atmospheric Pressure Argon Plasma Jet in Humid Air (J. Phys. D: Appl. Phys. 46 (2013) 275201)). *J. Phys. D. Appl. Phys.* **2014**, *47* (7), 079502–079505. DOI:10.1088/0022-3727/47/7/079502.
(46) Van Gaens, W.; Bogaerts, A. Erratum: Kinetic Modelling for an Atmospheric Pressure Argon Plasma Jet in Humid Air (J. Phys. D: Appl. Phys. 46 (2013) 275201)). *J. Phys. D. Appl. Phys.* **2014**, *47* (7). DOI:10.1088/0022-3727/47/7/079502.
(47) Tsang, W.; Hampson, R. F. Chemical Kinetic Data Base for Combustion Chemistry. Part I. Methane and Related Compounds. *J. Phys. Chem. Ref. Data* **1986**, *15* (3), 1087–1279. DOI:10.1063/1.555759.
(48) Atkinson, R.; Baulch, D. L.; Cox, R. A.; Hampson, R. F.; Kerr Chairman, J. A.; Troe, J. Evaluated Kinetic and Photochemical Data for Atmospheric Chemistry: Supplement III. IUPAC Subcommittee on Gas Kinetic Data Evaluation for Atmospheric Chemistry. *J. Phys. Chem. Ref. Data* **1997**, *18* (2), 881–1097. DOI:10.1063/1.555832.
(49) Hippler, H.; Rahn, R.; Troe, J. Temperature and Pressure Dependence of Ozone Formation Rates in the Range 1-1000 Bar and 90-370 K. *J. Chem. Phys.* **1990**, *93* (9), 6560–6569. DOI:10.1063/1.458972.
(50) Heimerl, J. M.; Coffee, T. P. The Unimolecular Ozone Decomposition Reaction. *Combust. Flame* **1979**, *35* (C), 117–123. DOI:10.1016/0010-2180(79)90015-4.
(51) Suzzi Valli, G.; Orrú, R.; Clementi, E.; Laganà, A.; Crocchianti, S. Rate Coefficients for the N+O2reaction Computed on an Ab Initio Potential Energy Surface. *J. Chem. Phys.* **1995**, *102* (7), 2825–2832. DOI:10.1063/1.468660.
(52) Baulch, D.L.; Cobos, C.J.; Cox, R.A.; Frank, P.; Hayman, G.; Just, Th.; Kerr, J.A.;

Murrells, T.; Pilling, M.J.; Troe, J.; Walker, R.W.; Warnatz, J. Evaluated Kinetic Data for Combusion Modelling. Supplement I. *J. Phys. Chem. Ref. Data* **1994**, *23*, 847–1033. DOI:10.1063/1.555953.

(53) Hjorth, J.; Notholt, J.; Restelli, G. No Title. *Int. J. Chem. Kinet.* **1992**, *24*, 51–65. DOI:10.1002/kin.550240107.

(54) Herron, J. T. Rate of the Reaction NO+N. *J. Chem. Phys.* **1961**, *35* (3), 1138–1139. DOI:10.1063/1.1701202.

(55) Bemand, P. P.; Clyne, M. A. A.; Watson, R. T. Atomic Resonance Fluorescence and Mass Spectrometry for Measurements of the Rate Constants for Elementary Reactions: O 3PJ + NO 2 → NO + O2 and NO + O3 → NO 2 + O2. *J. Chem. Soc. Faraday Trans. 2 Mol. Chem. Phys.* **1974**, *70* (02), 564–576. DOI:10.1039/F29747000564.

(56) Atkinson, R.; Baulch, D. L.; Cox, R. A.; Crowley, J. N.; Hampson, R. F.; Hynes, R. G.; Jenkin, M. E.; Rossi, M. J.; Troe, J.; Center, P. R.; Science, L. H.; Centre, T.; Park, S. Evaluated Kinetic and Photochemical Data for Atmospheric Chemistry: Volume I – Gas Phase Reactions of Ox, HOx, NOx and SOx Species. *J. Phys. Chem. Ref. Data* **2004**, *I*, 1461–1738. DOI:10.5194/acp-4-1461-2004.

(57) Tsang, W.; Herron, J. T. Chemical Kinetic Data Base for Propellant Combustion I. Reactions Involving NO, NO2, HNO, HNO2, HCN and N2O. **1991**, *20* (4). DOI:10.1063/1.555890.

(58) Graham, R.A.; Johnston, H. S. The Photochemistry of the Nitrate Radical and the Kinetics of the Nitrogen Pentoxide-Ozone System. *J. Phys. Chem.* **1978**, *82* (3), 254–268. DOI:10.1021/j100492a002.

(59) Ashmore, P.G.; Burnett, M. G. Concurrent Molecular and Free Radical Mechanisms in the Thermal Decomposition of Nitrogen Dioxide. *J. Chem. Soc. Faraday Trans. 2* **1962**, 253–261. DOI:10.1039/TF9625800253.

(60) Campbell, I. M.; Thrush, B. A. Behaviour of Carbon Dioxide and Nitrous Oxide in Active Nitrogen. *Trans. Faraday Soc.* **1966**, *62*, 3366–3374. DOI:10.1039/tf9666203366.

(61) Nighan, W. L. Electron Energy Distributions and Collision Rates in Electrically Excited N2, CO, and CO2. *Phys. Rev.* **1970**, *2* (5), 1989–2000. DOI:10.1103/PhysRevA.2.1989.

(62) Kossyi, I. A.; Kostinsky, A. Y.; Matveyev, A. A.; Silakov, V. P. Kinetic Scheme of the Non-Equilibrium Discharge in Nitrogen-Oxygen Mixtures. *Plasma Sources Sci. Technol.* **1992**, *1* (3), 207–220. DOI:10.1088/0963-0252/1/3/011.

(63) Beverly, R. E. Ion Aging Effects on the Dissociative-Attachment Instability in CO2 Lasers. *Opt. Quantum Electron.* **1982**, *14* (6), 501–513. DOI:10.1007/BF00610306.

(64) Whitaker, M.; Biondi, M.A.; Johnsen, R. Electron-Temperature Dependence of Dissociative Recombination of Electrons with N2^+. *Phys. Rev. A* **1981**, *24*, 743–745. DOI:10.1103/PhysRevA.24.743.

(65) Gudmundsson, J. T.; Thorsteinsson, E. G. Oxygen Discharges Diluted with Argon: Dissociation Processes. *Plasma Sources Sci. Technol.* **2007**, *16* (2), 399–412. DOI:10.1088/0963-0252/16/2/025.

(66) Ionin, A. A.; Kochetov, I. V.; Napartovich, A. P.; Yuryshev, N. N. Physics and Engineering of Singlet Delta Oxygen Production in Low-Temperature Plasma. *J. Phys. D. Appl. Phys.* **2007**, *40* (2), R25–R36. DOI:10.1088/0022-3727/40/2/R01.

(67) Cenian, A.; Chernukho, A.; Borodin, V. Modeling of Plasma-Chemical Reactions in Gas Mixture of CO2 Lasers. II. Theoretical Model and Its Verification. *Contrib. to Plasma Phys.* **1995**, *35* (3), 273–296. DOI:10.1002/ctpp.2150350309.

(68) Beuthe, T. G.; Chang, J.-S. Related Content Chemical Kinetic Modelling of Non-Equilibrium Ar- CO 2 Thermal Plasmas. *Jpn. J. Appl. Phys.* **1997**, *36* (4997), 4997–5002. DOI:10.1143/JJAP.36.4997.
(69) Eliasson, B.; Hirth, M.; Kogelschatz, U. Ozone Synthesis from Oxygen in Dielectric Barrier Discharges. *J. Phys. D. Appl. Phys.* **1987**, *20* (11), 1421–1437. DOI:10.1088/0022-3727/20/11/010.
(70) Mcfarland, M.; Dunkin, D. B.; Fehsenfeld, F. C.; Schmeltekopf, A. L.; Ferguson, E. E. Collisional Detachment Studies of NO-. *J. Chem. Phys.* **1972**, *56* (5), 2358–2364. DOI:10.1063/1.1677542.
(71) Adamovich, I. V.; MacHeret, S. O.; Rich, J. W.; Treanor, C. E. Vibrational Energy Transfer Rates Using a Forced Harmonic Oscillator Model. *J. Thermophys. Heat Transf.* **2008**, *12* (1), 57–65. DOI:10.2514/2.6302.
(72) Esposito, F.; Armenise, I.; Capitelli, M. N-N2 State to State Vibrational-Relaxation and Dissociation Rates Based on Quasiclassical Calculations. *Chem. Phys.* **2006**, *331* (1), 1–8. DOI:10.1016/j.chemphys.2006.09.035.
(73) Esposito, F.; Armenise, I.; Capitta, G.; Capitelli, M. O-O2 State-to-State Vibrational Relaxation and Dissociation Rates Based on Quasiclassical Calculations. *Chem. Phys.* **2008**, *351* (1–3), 91–98. DOI:10.1016/j.chemphys.2008.04.004.